Bending effect on the risk for delamination at the reinforcement/matrix interface of 3D woven fabric composite using a shell-like RVE

B. Piezel, B.C.N. Mercatoris, W. Trabelsi, L. Laiarinandrasana, A. Thionnet, T.J. Massart

This paper was published in Composites Structures, vol. 94(8), pp 2343-2357, 2012

Bending effect on the risk for delamination at the reinforcement/matrix interface of 3D woven fabric composite using a shell-like RVE

B. Piezel[a], B.C.N. Mercatoris[a], W. Trabelsi[b], L. Laiarinandrasana[b], A. Thionnet[b,c], T.J. Massart[a,*]

[a] *Building, Architecture and Town Planning Department CP 194/2, Université Libre de Bruxelles (ULB), Av. F.-D. Roosevelt 50, 1050 Brussels, Belgium*

[b] *MINES ParisTech, Centre des Matériaux, CNRS UMR 7633, BP 87, 91003 Evry Cedex, France*

[c] *Université de Bourgogne, Mirande, BP 47870, 21078 Dijon, France*

Abstract

This paper presents a computational homogenisation-based technique for flexural effects in textile reinforced composite planar shells. An homogenisation procedure is used for the in-plane and the out-of-plane behaviour of three-dimensional woven composite shells taking the in-plane periodicity of the material into account while relaxing any periodicity tying in the thickness direction. Several types of damage (matrix or reinforcement cracking, delamination, ...) can appear in a composite material. In this paper, material non-linear computations are used to assess the importance of bending on the risk for delamination at the reinforcement/matrix interface. The normal and tangential stresses at the interface are computed and a simplified criterion for delamination is used for this purpose. The effect of flexural loading on the stress components responsible for a potential delamination failure mode at the interface is analysed. The values of interface stresses obtained by means of flexural homogenisation are compared with 3D homogenisation results using periodicity constraints along the thickness direction, and compared qualitatively with experimental facts available from the litterature. The importance for taking flexural effects into account properly is emphasized.

*Corresponding author. Tel. : +32 2 650 27 42 ; Fax : +32 2 650 27 82
On leave at McGill University, Montreal, Canada
Email address: thmassar@ulb.ac.be (T.J. Massart)

Published in Composites Structures, vol. 94(8), pp 2343-2357, 2012 *February 1, 2014*

Keywords: woven composite, computational homogenisation, non-linear flexural behaviour, delamination, debonding, thermoplastic yarns

1. Introduction

Fibre-reinforced composite materials such as textile composites start nowadays being used as high performance structural materials for instance in automotive, aerospace and naval industrial applications. Due to their high stiffness and strength, for a rather low density and low cost manufacturing, two-dimensional woven composites were widely used in laminated composites such as plain, twill and satin weave fabrics. The development of new weaving techniques [1] allowed the emergence of complex three-dimensional woven reinforcements which offer a higher strength to delamination between plies than laminated composites due to the presence of reinforcing yarns in the through-thickness direction [2, 3]. The complex microstructural geometrical arrangement of such materials however renders the effective properties and the local stress fields under loading difficult to capture. In this contribution, a rather flexible material will be considered, which is made of polymeric three-dimensional woven composites, and which can be used for instance for transport purposes. The 3D woven composite will be considered as a thin structure which requires taking into account a shell assumption in structural computations. In such an application, the woven composite may be subjected to various loads of different nature, frequency and intensity, which are dominated by flexural effects, particularly when being pre-tensioned and bent around pulleys, or when subjected to impact loadings. In the former case, bending may therefore occur in the longitudinal warp direction whereas in the latter case, bending occurs in both the warp and weft directions. Based on the classical laminate theory, different simple micromechanical analytical approaches were developed to extract the effective elastic properties of such a microstructure by assuming geometrical simplifying assumptions for this microstructural arrangement. For the membrane behaviour, series and parallel mosaic models were proposed in [4] assuming discontinuous reinforcement, which neglects the reinforcement undulations. These undulations were taken into account by means of shape functions in enhanced models, see [5, 6, 7, 8]. For the out-of-plane behaviour, an analytical model was proposed in [9] to extract the membrane-flexural elastic stiffness coefficients.

When the geometry of the weave is more complex as for instance in three-dimensional woven composites [10], micromechanical analytical models do

not allow capturing correctly the structural properties since the microstructure is not explicitly taken into account, particularly the yarn undulations. Multi-scale frameworks combined with the finite element method were therefore developed to represent the complex microstructural geometry, leading to a better estimation of the global elastic properties [11], as well as the possibility to capture the local microstructural heterogeneous stress and strain fields [12, 13, 14, 15]. Thanks to the development of design tools dedicated to woven composites [16], and domain decomposition methods allowing the solution of problems with large numbers of degrees of freedom, finite element modelling is increasingly used for the modelling of three-dimensional woven composites, see for instance [17, 18, 19, 20]. A local damage analysis was recently proposed in [21] for satin weave composites under tensile loading using mesoscopic finite element simulations.

The structural non-linear behaviour of textured heterogeneous materials such as woven composites is difficult to capture, because of their complex microstructure and the interplay between different damaging mechanisms at the microstructural scale [22]. As a counterpart to their efficiency, phenomenological models may be complex to formulate and costly to identify due to a large number of material parameters, see for instance [23]. Analytical models based on geometrical assumptions were developped in [24, 25] for damaged two-dimensional woven composites accounting for transverse yarn cracking and interface debonding.

Different multi-scale techniques have been developed in the past decades allowing postulating closed-form constitutive laws at the scale of the constituents, on which the material parameters are a priori more straightforward to identify.

The asymptotic homogenisation theory, initially presented in [26, 27], is based on the assumption of a periodic microstructure and uses an asymptotic expansion of the macroscopic variables that allows defining a boundary-value problem on a representative volume element (RVE) for each order under consideration, see [28]. This technique is still widely used for composite materials, as shown in an extensive review [29]. The flexural behaviour identification of textile composites is even more complex since membrane-flexural couplings then need to be taken into consideration. A multi-scale approach accounting for such effects can therefore offer an alternative solution for the characterisation of such periodic heterogeneous materials. Methodologies were recently proposed for the modelling of shell-like heterogeneous structures such as laminated composites, honeycomb-type sandwiches or masonry

structures by means of multi-scale approaches extended to shell-like formulations. Unit cell asymptotic homogenisation techniques were used to determine the elastic properties of beam-like structures in [30], of composite shell structures with orthotropic reinforcements in [31], and of periodic running bond masonry walls subjected to out-of-plane loading in [32, 33].

Strongly coupled multi-scale strategies have been developped for heterogeneous materials in the case of a finite scale separation. In such substructuring approaches, the coupling is based on interface conditions on the element level between the different scales under consideration [34]. Based on a Voronoi cell model at the finest scale, an adaptative three-level methodology using an asymptotic homogeneisation procedure for the coupling between the scales was also proposed in [35] for damage assessment in two-dimensional composite materials. As an application, this approach was used for the modelling of damage-induced anisotropy in composites undergoing fiber-matrix interfacial debonding, see [36], recently enhanced by incorporating the effects of the loading history on the damage variables, see [37]. However, to the knowledge of the authors, the concept of substructuring models is not widely extended to shell formulation and loading conditions which is the focus of this paper.

Based on the scale separation assumption, computational homogenisation schemes were proposed allowing computing numerically the average non-linear material response of a heterogeneous microstructure by means of averaging theorems and a boundary-value problem on an RVE, see [38, 39, 40, 41]. This methodology also allows identifying the effective macroscopic properties of heterogeneous materials using off-line RVE computations, but can also be incorporated in two-scale computational nested schemes for structural computation known as FE^2. A critical review of the various micromechanical approaches was recently presented in [42] for simulating the macroscopic and microscopic responses of heterogeneous materials with spatially uniform microstructures, focusing on the concept of statistically representative volume element and on the use of the periodic unit cell within emerging homogenisation theories. The computational homogenisation approach was further extended for structured thin sheets using the homogenisation of a through-thickness RVE based on a second-order strategy, see [43, 44]. However, the thick shell case still raises questions concerning the transverse shear upscaling and remains a topic of current research, see [45]. A more restricted periodic homogenisation procedure was presented in [46] for the case of elastic Kirchhoff-Love masonry shells, and was recently extended for the non-linear out-of-plane behaviour of masonry walls taking into account cracking detec-

tion and propagation, see [47, 48].

The modelling of three-dimensional woven composite shells is a topic of current research particularly for the non-linear regime. The determination of elastic properties and failure behaviour of textile reinforced composites are vital for industrial design and engineering applications, a fact which is reflected in recent publications on this subject. A review of computational and analytical models for elastic and failure analysis of two-dimensional reinforced woven composites was presented in [49]. A discussion about the challenges and difficulties and a review of the available solutions to tackle the problem were recently presented in [50]. A computational homogenisation scheme was proposed to extract the flexural elastic coefficients of textile beams using an energy-based approach for the estimation of the transverse shear stiffness, see [51]. A common feature is that most of the current homogenisation approaches for the non-linear regime keep three-dimensional periodic tyings on unit cells, even for thin structures. As an illustration in [52] a comparison of different homogenisation methods was presented for the estimation of upper and lower bounds of the effective elastic properties for two-dimensional woven composites using three-dimensional periodic unit cells. These conventional mesoscopic finite element models for out-of-plane loaded laminated composites (making use of boundary value problems on a unit cell assuming periodicity in the thickness direction) can however drastically underestimate stress concentrations, especially in outer plies. Recent contributions [21, 53] presented a major step forward in this respect by relaxing the periodicity constraint in the thickness direction and investigating the corresponding effects for the in-plane loading of textile reinforced laminates. An iterative computational scheme based on an energy equivalence using enhanced boundary conditions for the modelling of free surface effects was used to extract the effective properties and to better evaluate the local stresses in the different plies of laminated woven composites.

The present contribution pushes forward this principle with a slightly different aim for 3D woven composites by exploiting a flexural homogenisation approach relaxing the periodicity in the thickness direction to determine the local stresses in a such composite shell, and to investigate their potential impact on delamination stresses.

The paper is structured as follows. The main ingredients of the in-plane periodic computational homogenisation scheme for thin planar shell properties are given in Section 2. The material considered in this contribution is presented in Section 3 with the adopted assumptions and mesoscopic con-

stitutive description. Section 4 deals with results of simulations using the proposed homogenisation strategy for the considered application, based on different loading cases and their combinations. A comparison with fully periodic 3D homogenisation is also given for in plane loading cases. These results are discussed in Section 5. The effect of the loading mode on the reinforcement/matrix delamination is more particularly studied. The paper is concluded in Section 6 by some final remarks and an outlook to future work.

2. Homogenisation of thin planar composite shells

The typical applications of a composite material can induce both in-plane tension-compression and flexural loading. As a result, the multiscale analysis of the composite requires accounting for both these effects, and should be performed with a shell type macroscopic kinematical description.

The microstructural material behaviour of constituents is upscaled computationally towards the membrane-flexural constitutive response of a thin shell by means of a computational homogenisation scheme. The principles of these upscaling relations were developed in [46] for the elastic membrane-flexural behaviour of thin planar masonry shells and used in [47, 48] for the non-linear cracking behaviour of such a heterogeneous material. They will be particularized here for the case of three-dimensional woven composites. Obtaining the average macroscopic response of a heterogeneous material from its underlying microstructure and the behaviour of its constituents can be based on the solution of a microstructural boundary value problem on a Representative Volume Element (RVE), relying on averaging theorems. A principle of scale separation between both scales of representation is used, which assumes that the material configuration is macroscopically homogeneous, but microscopically heterogeneous [40]. The crucial feature is here that a three dimensional through-thickness RVE is used to represent the microstructure. Considering the classical simplifying assumptions in engineering planar shell descriptions, the scale transitions need to be carefully derived [43, 44, 45]. Transverse shear effects at the macroscopic scale are neglected, and the computational homogenisation procedure proposed in [46, 47] is used here to take into account the material non-linearities of the three-dimensional woven composite. The approach described here is also applicable to stacked unit cells as published by Daggumati et al. [21, 53], provided the full thickness is included in the 3D through thickness RVE. However, treating such lami-

nates with a through thickness RVE as will be explained in the sequel would require heavy meshes. In that case, the approach proposed in [21, 53] seems largely preferable. A through thickness RVE is strongly suggested in the application presented in the present paper as a result of the 3D nature of the reinforcement. The approach is therefore complementary to the approach by Daggumati et al.

2.1. Averaging relations for Kirchhoff-Love planar shell kinematics

At the fine scale, a planar shell is represented by a prismatic through-thickness RVE, defined by its trace $\mathcal{S}_{\text{RVE}}$ on the reference surface of the shell and its thickness, corresponding to the shell thickness [43], see Figure 1. The averaging theorems linking the coarse (macro) scale and the fine (meso) scale quantities have to be verified for the strain, the stress and the work variation. For the case of the Kirchhoff-Love planar shell kinematics, it is postulated that the macroscopic membrane strain tensor $\mathbf{E}$ is the average of the local membrane strain tensor over the reference surface $\mathcal{S}_{\text{RVE}}$. The macroscopic curvature tensor $\boldsymbol{\chi}$ is assumed to be the surface average of the local curvature tensor over $\mathcal{S}_{\text{RVE}}$

$$\mathbf{E} = \frac{1}{\mathcal{S}_{\text{RVE}}} \int_{\mathcal{S}_{\text{RVE}}} (\vec{\nabla}\vec{u}_r)^{\text{sym}} \, \mathrm{d}\mathcal{S}_{\text{RVE}} \tag{1}$$

$$\boldsymbol{\chi} = \frac{1}{\mathcal{S}_{\text{RVE}}} \int_{\mathcal{S}_{\text{RVE}}} -\vec{\nabla}\vec{\nabla}u_z \, \mathrm{d}\mathcal{S}_{\text{RVE}} \tag{2}$$

where $\vec{u}_r$ and u_z are the in-plane and out-of-plane projections of the microstructural displacement vector, respectively, on the reference surface and in the thickness direction. The energy consistency between macroscopic and fine scale work variations is classically assumed, and expressed here by

$$\mathbf{N}:\delta\mathbf{E} + \mathbf{M}:\delta\boldsymbol{\chi} = \frac{1}{\mathcal{S}_{\text{RVE}}} \int_{\mathcal{V}_{\text{RVE}}} \boldsymbol{\sigma}:\delta\boldsymbol{\varepsilon} \, \mathrm{d}\mathcal{V}_{\text{RVE}} \tag{3}$$

where $\boldsymbol{\varepsilon}$ is the mesostructural infinitesimal strain tensor work conjugate to the mesoscopic stress field $\boldsymbol{\sigma}$, and $\mathbf{N}$ and $\mathbf{M}$ are respectively the macroscopic membrane force and bending moment tensors. Combining (1) and (3) with appropriate boundary conditions on the RVE leads to the satisfaction of the averaging theorem for the stress measures and allows relating the macroscopic membrane force tensor $\mathbf{N}$ and the macroscopic bending moment tensor $\mathbf{M}$ to the mesoscopic statically admissible stress field $\boldsymbol{\sigma}$ at the surface of the RVE.

2.2. Shell homogenisation with in-plane periodicity constraints

Computational homogenisation procedures for composite materials most often use periodic boundary conditions on each face of the RVE, including the top and bottom faces even though these should remain physically unconstrained when flexural effects are predominant, see [15]. The relaxation of the periodicity constraints in the thickness direction can however be required to better estimate local stresses, and thereby failure mechanisms such as delamination, matrix cracking or reinforcement cracking. Here, the homogenisation framework will be defined assuming periodicity of the microstructure in its plane only. In-plane periodic boundary conditions on RVEs were shown to provide a better estimation of the overall elastic properties than other boundary conditions (uniform displacements or tractions) for full two-dimensional or full three-dimensional cases, see [38, 40]. Suppressing the rigid body translations and rotations of the RVE, the kinematically admissible displacement field for macroscopic shell kinematics is strain-periodic and given by [54]

$$\vec{u}_r = \mathbf{E}\cdot\vec{x}_r + z\,\boldsymbol{\chi}\cdot\vec{x}_r + \vec{u}_r^{\,p} \tag{4}$$

$$u_z = -\frac{1}{2}\,\vec{x}_r\cdot\boldsymbol{\chi}\cdot\vec{x}_r + u_z^p \tag{5}$$

where $\vec{u}_r^{\,p}$ and u_z^p are in-plane and out-of-plane periodic displacement fluctuation fields, added to the average displacement field to account for the heterogeneity of the material. For such a displacement field, the averaging relations (1) are satisfied, and both fluctuation fields can be eliminated. The in-plane periodic boundary conditions can be prescribed on the RVE using tying relations between boundary points related by periodicity on the internal (in-plane) faces. These conditions are expressed in [46, 54] for the case of masonry and are particularised to the woven composite unit cell in the sequel. Note that relations (4) and (5) do not incorporate any constraint on the top and bottom faces of the RVE. Since the 3D woven composite considered here exhibits a periodic heterogeneous mesostructure, a unit cell, i.e. a single period RVE, is used to characterize the non-linear behaviour within a geometrically linear setting. A rectangular parallelepipedic through-thickness portion of the woven composite, as sketched in Figure 1 will be used as RVE.

The kinematically admissible displacement field assumed in the volume of the RVE is defined by Equations (4) and (5). Based on this assumption, the tying relations prescribing the in-plane periodic boundary conditions on the RVE are now detailed. Note that the following developments can be found

in [47, 55] for the case of running bond masonry for which periodicity vectors are slightly different.

Considering opposite internal boundaries of the RVE, and eliminating the periodic fluctuations $\vec{u}^{\,p}$ based on the in-plane periodicity argument, Equations (4) and (5) lead to the following expressions

$$\vec{u}_r^{+} - \vec{u}_r^{-} = (\mathbf{E} + z\,\boldsymbol{\chi})\cdot(\vec{x}_r^{+} - \vec{x}_r^{-}) \tag{6}$$

$$u_z^{+} - u_z^{-} = -\frac{1}{2}\,\boldsymbol{\chi} : (\vec{x}_r^{+}\vec{x}_r^{+} - \vec{x}_r^{-}\vec{x}_r^{-}) \tag{7}$$

which involve only the relative displacements and positions between any pair of boundary points related by in-plane periodicity. The superscripts + and − refer to the opposite parts of the internal surface of the RVE, see Figure 1 for the case of the three-dimensional woven composite.

2.3. Control system of the fine scale boundary value problem

The proper size and geometry of a RVE should be deduced from statistical considerations [56], or defined by the periodicity of a given microstructure. In the case of a small strain description, the Kirchhoff-Love generalised strains are given by six independent scalar quantities, i.e. the components of $\boldsymbol{E}$ and $\boldsymbol{\chi}$. The average deformed state of a RVE can therefore be fully prescribed using six displacements if in-plane periodicity is enforced. A possible choice for these six controlling displacements is given in Figure 1 for the case of the woven composite considered here. The macroscopic membrane deformations are prescribed using three reference plane displacements, while the macroscopic curvatures are fixed by three out-of-plane displacements. Using Equations (4) and (5) and the periodicity conditions, the relations linking the controlling displacements to the average coarse-scale strains measures read :

$$u_x^1 = lE_{xx} \tag{8}$$

$$u_y^1 = lE_{xy} \tag{9}$$

$$u_y^2 = hE_{yy} \tag{10}$$

$$u_z^1 = -\frac{l^2}{2}\chi_{xx} \tag{11}$$

$$u_z^2 = -\frac{h^2}{2}\chi_{yy} \tag{12}$$

$$u_z^3 = -\frac{l^2}{2}\chi_{xx} - hl\chi_{xy} - \frac{h^2}{2}\chi_{yy} \tag{13}$$

These relations can be written in a matrix form :

$$\{u_{\text{ctl}}\} = [D_u]^{-1}\{E_{\text{KL}}\} \tag{14}$$

where $\{u_{\text{ctl}}\}$ is a column vector of the six controlling degrees of freedom, $\{E_{\text{KL}}\}$ is a column vector of the Kirchhoff-Love generalised strains, and $[D_u]$ is a matrix which depends on the in-plane dimensions of the RVE reflecting relations (6) and (7). Considering (4), (5) and (3), the average Kirchhoff-Love stresses can be obtained from the controlling forces conjugate to the controlling displacements which represent the action of the neighbouring cells, [47]. The relations between these controlling forces and the generalised stresses are given by :

$$N_{xx} = \frac{1}{h} f_x^1 \tag{15}$$

$$N_{yy} = \frac{1}{l} f_y^2 \tag{16}$$

$$N_{xy} = \frac{1}{2h} f_y^1 \tag{17}$$

$$M_{xx} = -\frac{l}{2h} f_z^1 - \frac{l}{2h} f_z^3 \tag{18}$$

$$M_{yy} = -\frac{h}{2l} f_z^2 - \frac{h}{2l} f_z^3 \tag{19}$$

$$M_{xy} = -\frac{1}{2} f_z^3 \tag{20}$$

In a matrix form, this can be denoted

$$\{\Sigma_{\text{KL}}\} = [D_f]\{f_{\text{ctl}}\} \tag{21}$$

where $\{f_{\text{ctl}}\}$ is a column vector of the six controlling forces, $\{\Sigma_{\text{KL}}\}$ is a column vector of the Kirchhoff-Love generalised stresses, and $[D_f]$ is a matrix which depends on the in-plane dimensions of the RVE.

Based on Equations (14), any average deformation path can be prescribed. The related mesostructural boundary value problem is completely defined from the prescribed controlling degrees of freedom and the periodicity boundary conditions, and can be solved using a classical finite element scheme, provided mesostructural constitutive laws are postulated. This type of control is used in multi-scale nested scheme using displacement-based finite element schemes (FE^2 methodology), [40, 57, 58]. It is emphasized that even though

no nested FE^2 multiscale simulation is performed here, the framework makes use of scale transition operators which are strictly equivalent to the ones used in FE^2 strategies, in the sense developped by [40] for 2D problems. Based on the in-plane periodicity assumption, the link defined between macroscopic strains and displacements at control points of the RVE, and between macroscopic stresses (and bending moments) and tying forces at these points on the RVE can be used to extract the homogenised tangent stiffness required in FE^2 simulations. Even though this macroscopic tangent stiffness is not extracted here, the basic principles of computational homogenisation are applied. Note that this Kirchhoff-Love planar shell computational homogenisation scheme can be connected to the general second-order solid-solid computational homogenisation framework developed in [59]. Such a link was established for the Reissner-Mindlin case by introducing the shell kinematical assumptions in the macroscopic second-gradient continuum, see [43] for more details. Note that the present framework to be used to extract computationally the flexural properties of the shell. Note also that the periodicity relaxation in the thickness direction is pursued with a different approach and with different objectives from the one presented by Ivanov et al. [53]. In the approach by Ivanov et al., a stacking of plies is considered with in-plane loading. A RVE representation of each ply is considered, and the boundary conditions applied on such RVEs are made non classical in order to account for a different response of plies located near the free surface in the thickness direction with respect to plies located near the mid-thickness. In our approach, the composite is assumed to be loaded by bending terms as well, and a result, a through thickness RVE is used. This is made mandatory by the fact that the underlying microstructure is a 3D woven composite (not a laminate). The scale transition operators are therefore different and complementary between both approaches: the approach in [53] seems more efficient for laminates, while the through thickness RVE allows treating 3D reinforcements (at the expense of larger computational times).

3. Problem statement and considered materials

3.1. Considered 3D woven composite internal structure

Any 3D woven composite can be treated for bending effects with the proposed framework. The material used in this contribution for the sake of illustration is typically used in transport moving strips, to transport various types of materials. It usually consists of several layers of polymeric materials.

The middle layer is of more particular interest in this paper and consists of a 3D woven composite. This composite material is covered above and below by a layer of polyvinyl chloride (PVC) and a layer of rubber.

The woven composite considered in this paper is a three-dimensional woven fabric embedded in a PVC matrix with a thickness of 9 mm. Since PVC presents an important viscosity in the molten state unlike epoxy resins commonly used in composites [60, 61, 62], the fabric is not impregnated by the matrix during the manufacturing process. The yarns will therefore be assumed dry in the sequel. The textile is composed of polyethylene terephthalate (PET) fibres for the warp yarns and polyamide 6-6 (PA66) fibres for the weft yarns. Three scales of interest can be considered for such woven composites (Figure 2). At the macroscopic scale, the composite can be considered as an orthotropic homogeneous shell. The mesoscopic scale allows taking the geometry of the fabric into account considering the yarns as transversly isotropic materials in an average sense. At the microscopic scale, the yarns consist of twisted assemblies of parallel fibre bundles. In this paper, the influence of the various macroscopic loading modes on the potential competition between failure mechanisms at the mesoscopic scale is emphasized by scrutinising the influence of bending and representing the effects at the microscopic scale collectively in phenomenological laws. Other damage mechanisms like matrix or fibre damage experimentally observed in [63] are not studied here, but the potential increase of delamination risk as a result of bending is analysed. The homogenisation of thin planar shells could be used to study these mechanisms as well in subsequent studies. The woven mesostructure, assumed to be periodic, has been identified by means of optical analyses of through-thickness sections, see Figure 3. The repeating pattern of the three-dimensional woven fabric is sketched in Figure 4. It consists of four horizontal planes of weft yarns and four vertical planes of warp yarns. The number of weft yarns interleaving between two successive warp yarns is therefore equal to four. The warp yarn intercepts the yarns of weft on two consecutive planes of weft yarns. Finally, the periodic pattern consists of four vertical planes of warp yarns in the weft direction. The longitudinal direction of the composite shell, is the warp direction of the woven fabric (denoted x in Figure 1), and is the transverse direction to the weft direction (denoted y in Figure 1).

3.2. Mesoscopic constitutive description

The mechanical behaviour of each constituents, i.e. warp yarns, weft yarns and matrix, is the same as reported in [63, 64]. In the present contribution, we neglect the variations of yarns properties induced by their own strain [65, 66] and a purely isotropic behaviour is assumed for the matrix. Moreover, the potential non-linearities due to the variation of waviness are neglected. The deformations are thus assumed too small to induce geometrical non-linearities at the macroscopic scale.

The non-linear behaviour of the reinforcement was characterised experimentally by tensile tests [63, 64]. Due to the complexity of such tests, the experimental characterisation was not performed at the fibre level, but at the level of the assembled yarns. This is further motivated by the fibrous nature of the yarns and by the twisted assembly of the bundles, which in any case makes it difficult to estimate the yarn global properties by homogenisation approaches, should the fibres properties and interactions be known. The global tensile behaviour of yarns is reported in Figure 5. It can be split into three domains: (i) an elastic domain, (ii) a second domain corresponding to a stiffening of the yarns, and (iii) a third domain corresponding to the reduction of the tangent modulus up to the failure of the yarns. This third stage is disregarded in the present study. This complex behaviour of the yarns originates from geometrical and material non-linearities taking place at the microscopic level. The twisted configuration of the fibre bundles induces non-linear couplings between the longitudinal and transversal behaviours. In addition, tensile tests on single thermoplastic fibres were performed in [67, 68, 69, 70, 71] showing a correlation between the stiffness increase and the degree of cristallinity. This can be explained by an alignment of amorphous macromolecules in the direction of loading. The increase of stiffness observed during the monotonic tensile tests can be modelled with an elastoplastic behaviour with two isotropic hardening terms [72, 73]. The deformation of the material is divided additively into two parts :

$$\boldsymbol{\varepsilon} = \boldsymbol{\varepsilon}_e + \boldsymbol{\varepsilon}_p \tag{22}$$

where $\boldsymbol{\varepsilon}_e$ is the elastic part of the total strain and $\boldsymbol{\varepsilon}_p$ is the plastic strain. The plastic yield function is defined as :

$$f(\boldsymbol{\sigma}, R) = J(\boldsymbol{\sigma}) - R(p) \tag{23}$$

where J is the second invariant of stress deviator $\boldsymbol{s}$ defined by the equation:

$$J = (\frac{3}{2}\boldsymbol{s} : \boldsymbol{s})^{\frac{1}{2}} \tag{24}$$

R is a scalar variable defining the isotropic hardening of material as :

$$R = R_0 + Q(1 - e^{-bp}) + A(e^{Bp} - 1) \tag{25}$$

where p is the cumulated effective plastic strain, and R_0, Q, b, A and B are material parameters to be identified. R_0 is the initial yield stress. The increase of tangent modulus with plastic strain is given by the second isotropic hardening contribution in Equation (25). These five parameters can be obtained by inverse methods based on the tensile tests performed on yarns (Figure 5) and from the results of tensile tests carried out on the composite material itself as presented in [63, 64]. With the fine scale parameters presented in Table 2, tensile tests on the composite material in the warp yarn direction can be represented fairly well with the shell homogenisation framework presented in Section 2. This is illustrated in Figure 6 by means of the membrane stress-strain response of the composite and of the corresponding homogenised tangent stiffness evolution.

Further, due to their fibrous microstructure, the transverse behaviour of the yarns is more difficult to characterize experimentally. For the case of impregnated yarns, a homogenisation procedure and an empirical model were compared in [15, 74] regarding the homogenised elastic stiffness of a yarn. With a matrix volume fraction in the yarns equal to 0.05 and using formulae proposed by [15, 74] with a fibre modulus approximated from the full yarn tensile tests in Figure 5, a ratio between the longitudinal and the transverse moduli of about 150 is found. In the present contributions in which dry yarns are considered, a ratio of 100 between both moduli will be chosen in order to capture the anisotropy of the elastic behaviour of yarns. Note that the range of values of such a ratio can be quite broad as shown in the literature. Boisse et al. proposed a a ratio between 20 for dry carbon yarns [75] and 13 000 for dry glass yarns [65]. A variation of this ratio will therefore be examined for one of the loading cases in the unit cell computations presented in the sequel (see Section 4).

For the sake of simplicity, the model presented above will be assumed isotropic for the plastic part and transversly isotropic for the elastic part.

It is noted that it is crucial to distinguish the anisotropy of the yarns behaviour at the mesoscopic scale, and the anisotropy of the composite be-

haviour at the macroscopic scale resulting from the difference of Young modulus of warp and weft yarns (material anisotropy) and the difference of the fabric pattern in warp and weft directions ('geometrical' anisotropy). The values of the parameters considered for the simulations are summarized in Table 2.

	E_x (MPa)	$E_y = E_z$ (MPa)	G_{xy} (MPa)	ν_{xy}	ν_{yz}
Warp yarns	15000	150*	15	0.1	0.05
Weft yarns	2996	30*	15	0.1	0.05
Matrix	400	0.3			

Table 1: Transversly isotropic elastic parameters of yarns for 3D woven composite RVE computations. The values of the transverse moduli marked by * were estimated with a ratio 100 as explained above.

	R_0 (MPa)	Q (MPa)	b	A (MPa)	B
Warp yarns	59	63	363	5.45	53.4
Weft yarn	5.6	15.34	403	7.4	68.9

Table 2: Material parameters for the reinforcement of the 3D woven composite RVE computations obtained from the fitting of the tensile tests performed on the composite (Figure 6).

3.3. Potential delamination issues in 3D woven composites

Given the type of microstructure, it is crucial to evaluate and to analyse the potential initiation of damage when the composite is subjected to loading cases incorporating flexural effects. Different damage modes can appear in woven composites such as matrix transverse and longitudinal cracking, interply delamination and reinforcement/ matrix debonding. Since the transverse stiffness can be affected by interfacial debonding, the potential for such a mechanism will be scrutinised here depending on the loading mode and on boundary conditions applied to the RVE (3D through-thickness periodicity homogenisation vs. shell kinematics homogenisation as presented in Section 2).

The mechanical behaviour of the interfaces between the reinforcement and the matrix has been studied by many authors. It has been shown in

[76, 77] that the interfacial debonding properties depend on the loading mode and more particularly on the relative importance between mode I and mode II in the stress state. However, only the influence of the shear stress on the interfacial debonding has been considered in most cases [78, 79, 80]. Most often, the pull-out test is used to extract the interfacial shear strength. It consists of extracting a fibre initially embedded in a matrix by tension and in measuring the force needed to pull-out the fibre assuming a constant shear stress distribution along the fibre. However, in a woven composite, the shear stress field is not constant due to the undulation of yarns and the interaction between adjacent yarns. An original test was proposed in [76] to measure the critical stress level for delamination for a mixed mode loading. This test combines a shear stress and a radial tensile stress at the interface between the fibre and the matrix. Such tests show that the contribution of a positive normal stress decreases the amount of shear stress needed to obtain a fibre/matrix debonding, making it important to take into account both the normal and the shear stress components at the interface to properly predict the debonding.

The criterion can generally be described by using local quantities:

$$\text{If } F(\sigma(\vec{x})) \geq 0 \rightarrow \text{debond with } \vec{x} \in \text{interface} \tag{26}$$

where F is the form of which depends on the complexity of the model used.

The following criterion was proposed in [81]:

$$\max(\sigma_{nn}, \tau_{eq}) \geq \sigma^{Y-\text{interface}} \rightarrow \text{debond} \tag{27}$$

with $\sigma_{nn} = |\vec{n}.\boldsymbol{\sigma}.\vec{n}|$,$\tau_{eq} = |\vec{n}.\boldsymbol{\sigma}.\vec{a}|$ and $\vec{n}.\vec{n} = 1$, $\vec{a}.\vec{a} = 1$, $\vec{a}.\vec{n} = 0$, where $\vec{n}$ and $\vec{a}$ are the unit normal and unit tangent vectors respectively, and $\sigma^{Y-\text{interface}}$ is the interface strength between the reinforcement and the matrix. A quadratic form for the debonding criterion was proposed in [82, 83].

Here, a simplified local stress criterion will be adopted to assess potential delamination initiation, based on the delamination stress state, defined as:

$$\sigma_{delamination} = \sqrt{\sigma_{nn}^2 + \alpha\tau_{eq}^2} \leq \sigma^{Y-\text{interface}} \tag{28}$$

where σ_{nn} is the stress component normal to the interface (peeling stress), where $\tau_{eq} = \sqrt{\tau_{rt}^2 + \tau_{st}^2}$ is the modulus of the tangential projection of the stress vector at the interface (see Figure 7), and where α is a coefficient

accounting for the relative contribution to failure of the interface of mode-I and mode-II stress components, that will be chosen as 0.5 here for the purpose of illustration. Note that only the distribution of the quantity defined by relation (28) will be analysed here for damage initiation, without explicitly modelling the progressive degradation of the interface properties, i.e. without representing delamination propagation, which would require cohesive zones at the interface.

4. Mesoscopic unit cell computations

4.1. Meshing and problem statement

Because of the complexity of the fabric pattern, meshing tools dedicated to woven composite were used. First, a geometrical model was created using the Wisetex software [15, 16]. This requires information in particular on the pattern of fabric, the shape and the dimensions of yarns, and the size of the periodic pattern. This model was then transferred into the FETex software [15]. The meshing of the periodic cell was performed using the ANSYS FE code [15, 63]. Periodicity relations had to be imposed on the faces of the cell which requires consistent meshes on opposite in plane faces of the RVE. The mesh obtained can then be transferred to the ZeBuLoN FE code [84] developed by MINES ParisTech. Computations were carried out with ZeBuLoN using the constituve equations presented in Section 3.2. The elements composing the mesh of yarns and matrix are quadratic tetrahedral elements with a 4 points integration scheme. The final mesh is shown in Figure 11 and contains 383,320 nodes, i.e. 1,149,960 degrees of freedom and 276,609 quadratic tetrahedral elements.

The effect of the loading mode on the potential delamination failure mechanism of textile reinforced composites will here be assessed by means of cell computations assuming that the composite shell is used in a transport moving strip type application. In order to deduce macroscopic average deformations to apply on the unit cells, typical loading modes of such a transport moving strip will be considered. First , the RVE is subjected to an in-plane longitudinal elongation (in the warp direction) corresponding to the typical pre-tension applied for the considered application. In addition to this in-plane tension, the RVE is subjected to a longitudinal bending to model such a composite sheet passing on a conveyor pulley, see Figure 8. It is assumed that the pre-tension applied is such that average longitudinal strain reaches a value of $E_{xx} = 0.0018$. For the longitudinal flexural effect, it is assumed that

the composite is bent around a conveyor pulley with a radius of 200 mm, which sets the curvature to be applied on the RVE given its thickness. The RVE computations presented below match these two imposed macroscopic strains.

Practically, the composite is also subjected to bending in the transversal or weft direction to keep the transported materials on the belt. This bending may be obtained with troughing idlers as sketched in Figure 8. To obtain the corresponding value of curvature χ_{yy} to be applied on the RVE, the bending of the composite in the weft direction is computed at the macroscopic scale with a shell description [63]. The maximal strain obtained is used to compute the curvature χ_{yy}, assuming a homogeneous elastic behaviour at the macroscopic scale. The value of maximal strain in this case is 0.07 which matches a curvature χ_{yy} of 0.0151.

Finally, bending occurs in both the warp and weft directions during any vertical impact loading. This loading depends of several factors such as the mass and the shape of impactor, or the heigth of fall. This loading is more complex to analyse than the one induced by the composite passing around the conveyor pulley, since bending along both types of yarns (warp and weft) then needs to be considered. To approximate this loading mode, the assumption is made that the curvature in the weft direction is the same as the one obtained when passing on the troughing idlers. The pre-tension in the warp direction is also considered. The value of curvature χ_{xx} evaluated is 0.004. All these loading cases are summarised in Table 3.

Note that all stress distributions at the interface between the yarns and the matrix are produced with 'capped' colorbars in the sequel in order to allow an easy comparison between the different figures. As a result of this capping, the peak values reported in the text are not explicitly seen on the figures.

4.2. In plane pre-tension along warp direction (LM1)

As a first illustration, the results of a simulation on a cell loaded by loading mode LM1 (Table 3) are reported on Figure 9. The contributions of each stress component introduced in (28) for the yarns in the warp direction are depicted in Figure 9 (a single layer of yarns is plotted to ease interpretation). In this case, the peeling stress σ_{nn} remains limited to 1.51 MPa and the maximal shear stress τ_{eq} is 5.06 MPa. The delamination stress defined in equation (28) reaches a value of 3.89 MPa, and it is maximal at the extrados of the undulation of the warp yarns that are located closest to the neutral

	physical description	E_{xx}	E_{yy}	χ_{xx}	χ_{yy}	type of BC
LM1	Pre-tension	0.0018	0	0	0	shell
LM2	tension	0.025	0	0	0	shell
LM3	bending around pulley	0.0018	0	0.005	0	shell
LM4	Transversal bending	0.0018	0	0	0.0151	shell
LM5	Vertical impact	0.0018	0	0.004	0.0151	shell

Table 3: Loading cases considered for 3D woven composite RVE computations. The types of boundary conditions denotes the type of kinematical assumption (shell = no thickness periodicity, 3D = thickness periodicity).

fibre of the shell. These values as such remain in a limited range and cannot evidently give rise to delamination.

Now, when the same loading is applied on an RVE with periodicity tyings applied in the thickness direction (3D homogenisation), the peeling stress σ_{nn} reaches a value of 1.58 MPa, while the maximal tangential stress τ_{eq} value is equal to 5.14 MPa. The delamination stress reaches 3.96 MPa. The maximal stresses at the interface are thus similar for the two types of boundary conditions. The addition of thickness periodicity seems to slightly over-constrain the RVE but in a negligible manner for the considered loading case. Moreover, no peak of maximal stresses is observed on weft yarns in this case. The maximal stresses zone on the warp yarns are also more extended in this case.

4.3. Flexural loading case along warp yarns (LM2 and LM3)

The most often used methods of homogenisation do not allow taking into account the flexural effects. In such cases, some contributions evaluate the maximal longitudinal strain associated to bending (as if the shell was homogeneous), and apply this strain as an average (uniform) in-plane membrane strain to the RVE [63]. For the sake of subsequent comparison, the RVE is subjected to an in-plane tension corresponding to this maximal strain associated to bending.

The shell RVE is subjected to an in-plane tension corresponding to the maximal bending strain computed when the composite is bent around a conveyor pulley using the loading mode LM2 (Table 3). Figure 10 depicts the peeling and delamination stresses, under this pure 'fake' tension case with shell boundary conditions (no thickness periodicity). The peeling stress

σ_{nn} reaches a value of 16.47 MPa, while the maximal tangential stress τ_{eq} value is equal to 29.11 MPa. The delamination stress defined in (28) reaches 25.48 MPa. As in the loading mode LM1, the maximal delamination stress is reached at the extrados of the undulation of the warp yarns located closest to the neutral fibre of the shell. When the same procedure is applied with a RVE with thickness periodicity, the peeling stress σ_{nn} reaches a value of 18.63 MPa, while the maximal tangential stress τ_{eq} value is equal to 29.35 MPa. The delamination stress reaches 26.46 MPa at the same locations. The maximal stresses at the interface thus reachs similar values for the two types of boundary conditions.

In order to properly study the influence of the loading mode on the peeling and delamination stresses, flexural loading mode in the warp direction with shell boundary conditions is next added to the real pre-tension, assuming proportional loading between membrane and flexural effects for the sake of simplicity (loading mode LM3). A curvature is added with the value $\chi = \frac{1}{R}$, where R is the radius of the pulley over which the composite is bent, see Figure 8. Figure 11 denotes the corresponding (amplified) deformed shape of the RVE, while Figure 12 depicts the various stress components entering relation (28). Due to the flexural effect captured by the shell homogenisation, the peeling stress σ_{nn} now reaches a maximal value of 7.4 MPa, while the equivalent tangential stress reaches 18.32 MPa. The maximum value of the equivalent stress entering the delamination criterion is 13.32 MPa. When compared to the values obtained with in plane pre-tension in Section 4.2, this means that these delamination stress levels are multiplied by almost a factor 3.5 due to the flexural effect with respect to in-plane pre-tension only. However, the location of the maximal delamination stress is still the same as the loading modes LM1 and LM2.

4.4. Other bending loading cases (LM4 and LM5)

Now, results of computations for various additional loading cases are shown to feed the discussion related to the influence of the direction of loading. In fact, such a 3D woven composite is subjected to bending not only in the warp direction but also in the weft direction. Flexural loading in the (transversal) weft direction may be used to maintain the transported materials on the composite shell (loading mode LM4), as well as during the vertical impact of minerals (loading mode LM5).

Figure 13 depicts the contributions of each stress component under loading LM4. The value of peeling stress reaches 13.7 MPa while the maximal

shear stress is 10.4 MPa. The delamination stress reaches 14.5 MPa and is located on the undulations closest to the free surface of the shell. It is emphasized that even for anisotropic yarns, the level of delamination stresses remains sufficiently high to raise the concern of delamination.

Finally, we present in Figure 14 the results of computations for a vertical impact of transported materials on the composite (loading mode LM5), combining pretension with both curvatures. The value of peeling stress is 14.4 MPa, the tangential stress is 15.6 MPa, while the delamination stress reaches 15.8 MPa on the undulation closest to the free surface of the shell.

5. Discussion

The presented results show that it is important to take into account the flexural effects to study the potential delamination damage in the composite material. The stress level at the interface is a consequence of the mismatch between the properties of yarns and matrix, more particularly the transversal properties of yarns. Moreover, the waviness of the reinforcement increases the complexity of the stress distribution and makes interpretations difficult.

The incorporation of bending in the warp direction along with the pretension strongly increases the delamination stress at the interface between the yarns and the matrix in a such description. The incorporation of the flexural effect may therefore play a crucial role in the competition between delamination and other damaging processes.

The above mentioned results show that the loading mode has an important effect on the stress state and more particularly on the stress state at the yarns/matrix interface. For a same maximal strain level at the macroscopic scale deduced from geometrical constraints from the composite loading conditions, the local shear and normal stress components on the interface are found to be much more severe for a flexural load than a uniform tensile load. If damage by delamination is likely to appear in the composite material studied here, it is important to take into account the flexural effects.

The results of the analysis can be compared qualitatively with experimental data from different authors [79, 85, 86, 87, 88]. These data indicate that the critical interfacial stress state (interfacial shear strength) depends on the relative Young moduli postulated for the yarns and for the matrix, but also on the interface adhesion (lubricating, surface roughness, ...) between them. The experimental values obtained in the litterature depend on the characterisation method. No experimental data is available for the effect of the surface

state of yarns. Only the ratio between the Young moduli of the yarns and the matrix is therefore used here. In [86], the values of shear strength are obtained from pull-out tests, but on single fibres. Yue et al. [86] measured the interfacial shear strength for different fibre/matrix systems with a ratio between 0.001 and 0.5. In the present manuscript, the value of R is about 0.0267 (for the warp yarn in the longitudinal direction and the matrix). According to [86], the corresponding interfacial stress strength should be about 15 MPa. For a polypropylene/glass fibre system, the modulus ratio and the interfacial strength are 0.0233 and 4.3 MPa respectively [87]. Pull-out tests were also performed by Miller et al. [85] on Epoxy/Kevlar fibres, with a moduli ratio between 0.0563 and 0.0726 and an interfacial shear strength between 22 and 44 MPa. Chua and Piggott [79] studied polyester/glass fibre and Epoxy/glass fibre systems. For such polyester matrix and a ratio equal to 0.0250, the interfacial shear strength reached 9.6 MPa; while for an Epoxy matrix, the modulus ratio is 0.0383 and the interface shear strength reached 13.6 MPa. In summary, based on these informations, for the composite used as an illustration in the present work, the interfacial shear strength should range between 5 and 15 MPa. If we compare this range of critical values with the maximal values obtained with different load cases, the interfacial shear strength can clearly be reached for flexural loading cases (cases LM3 to LM5). More particularly, it is seen from the results that the increase of the delamination stress is mainly related to the tangential component of the stress vector at the interfaces. If the composite is subjected only by the pretension, the stress levels at the interface between the yarns and the matrix show that delamination is not really an issue.

The stress state at the interface is actually not a pure shear stress, since normal stresses are also present. Watson and Clyne [76] showed that presence of normal stresses during a pull-out test decreases the interfacial shear strength. To illustrate this, Figure 15 depicts the so-called phase angle ψ [76] , defined as the angle between the tangential component of the stress vector and the stress vector at the interface. ψ is between $-90°$ for a pure compression normal loading and $90°$ for a pure tensile normal loading. A pure shear loading is obtained for a an angle equal to $0°$. This value can be considered as a ratio between mode I and mode II loading. The zones subjected to peeling stresses ($\psi = 90°$) are slightly more extended in the case of bending than in the case of tension. However, as expected, the yarns located closest to the neutral axis of the shell are not subjected to tensile peeling stresses, which shows that the flexural effect has to be taken into account to properly

determine the positions for potential delamination. This clearly indicates that the mode I is dominant where bending is taken into account while the mode II is the most important for an in-plane tension load. Moreover, the shear and the tensile zones are differents for flexural or tensile loads.

Transverse elastic properties are difficult to estimate as already discussed in Section 3.2. The effect of a change in the transverse Young modulus of the yarns is therefore analysed here. The ratio of the yarns longitudinal modulus to the transverse one is therefore varied in the range [1 .. 1000]. The normal and tangential stress at the interface between the yarns and the matrix with these ratios are depicted in Figure 16. The normal (peeling) stresses σ_{nn} are rather limited for all the realistic values of the ratio. Peak values from 7.13 MPa for $E_L/E_T = 1000$ to 10.94 for $E_L/E_T = 10$, while only a unit ratio (yarns assumed to behave with isotropic properties) leads to important peak values of 22.5 MPa on the warp yarns interfaces (unrealistic values are found for the weft yarns as a result of insufficient discretisation). Quite expectedly, the tangential component of the stress at the interface on the contrary seems much less affected by the ratio of the moduli, as its peak value ranges from 18.18 for $E_L/E_T = 1000$ to 18.46 MPa for $E_L/E_T = 10$. A unit ratio of the moduli leads to a peak value of 22.64 MPa. These results seem to confirm that the potential delamination is still present independently from the relative Young moduli of transversly isotropic yarns. Of course, further research is required both from an experimental and computational viewpoint to confirm this. In particular, future efforts related to the effect of anisotropy in the non-linear characteristics of the yarns would be of interest.

6. Conclusions

A shell computational homogenisation scheme was presented and applied to a 3D woven composite. Based on a generalisation of periodic homogenisation, scale transitions were presented which allow using through-thickness 3D RVEs to extract the average response of heterogeneous shells with complex microstructures. These scale transitions can take into account flexural effects and their coupling with in-plane loading while relaxing any constraint between the top and bottom faces of the shell. This computational homogenisation framework was used to study the possibility for yarns/matrix delamination and its sensitivity to bending loading. Normal and tangential stresses at the yarns/matrix interface were computed for different types of loading (tensile and bending). A strong influence of the loading mode on

the delamination stresses was shown to appear for such 3D woven composites. In particular, a flexural loading induced an increase of normal and shear at the yarns/matrix interface. Furthermore, this increase was shown to be dependent on the nature of the considered reinforcement (monolithic vs fibrous yarns). These values were compared with experimental range of values obtained by different authors. The results suggest that bending can participate to induce a local delamination at the interface and should not be disregarded in subsequent studies. Moreover, a parameter called phase angle ψ has been defined, indicating the local ratio between mode I and mode II at the interface for each studied loading mode. It is emphasized that the computational methodology introduced here is very general and it can be employed for different types of composite and various industrial applications [1, 89]. Moreover, the delamination is not the only damage that can appeare in a composite material. Future efforts will be directed at combining delamination propagation under flexural effects with matrix and yarns damages, which have been observed experimentally in [63].

Acknowledgement

The scrutiny of the reviewers which lead to a substantial improvement of the manuscript is gratefully acknowledged. The support from F.R.S-FNRS Belgium for intensive computational facilities through grant 1.5.032.09.F is also acknowledged. The last author is grateful for the facilities provided by the Environmental Geomechanics group, Department of Civil Engineering and Applied Mechanics, McGill University.

References

References

[1] A.P. Mouritz, M.K. Bannister, P.J. Falzon, and K.H. Leong. Review of applications for advanced three-dimensional fibre textile composites. *Composites: Part A*, 30:1445–1461, 1999.

[2] B. Sun, B. Gu, and X. Ding. Compressive behavior of 3-d angle-interlock woven fabric composites at various strain rates. *Polymer testing*, 24:447–454, 2005.

[3] C. El Hage. *Modélisation du comportement élastique endommageable de matériaux composites à renfort tridimensionnel*. PhD thesis, Université de Technologie de Compiègne, 2006.

[4] T. Ishikawa. Anti-symmetric elastic properties of composite plates of satin weave cloth. *Fibre Science and Technology*, 15(2):127–145, 1981.

[5] T. Ishikawa and T.W. Chou. Stiffness and strengh behaviour of woven fabric composites. *Journal of Materials Science*, 17(11):3211–3220, 1982.

[6] T. Ishikawa and T.W. Chou. Elastic behaviour of woven hybrid composites. *Journal of Composite Materials*, 16(1):2–19, 1982.

[7] N.K. Naik and P.S. Shembekar. Elastic behavior of woven fabric composites : I-lamina analysis. *Journal of Composite Materials*, 26(15):2196–2225, 1992.

[8] N.K. Naik and P.S. Shembekar. Elastic behavior of woven fabric composites : II-lamina analysis. *Journal of Composite Materials*, 26(15):2226–2246, 1992.

[9] P. Chaphalkar and A.D. Kelkar. Classical laminate theory model for twill weave fabric composites. *Composites Part A-Applied Science and Manufacturing*, 32(9):1281–1289, 2001.

[10] S.V. Lomov, A.V. Gusakov, G. Huysmans, A. Prodromou, and I. Verpoest. Textile geometry preprocessor for meso-mechanical models of woven composites. *Composite Science and Technology*, 60:2083–2095, 2000.

[11] A.G. Prodromou, S.V. Lomov, and I. Verpoest. The method of cells and the mechanical properties of textile composite. *Composite structures*, 93:1290–1299, 2011.

[12] P. Paumelle, A. Hassin, and F. Lene. Microstress analysis in woven composite structure. *Recherche Aérospatiale*, 6:47–62, 1991.

[13] J.M. Guedes and N. Kikuchi. Preprocessing and postprocessing for materials based on the homogenization method with adaptative finite element methods. *Computer Methods in Applied Mechanics and Engineering*, 83:143–198, 1990.

[14] J.D. Whitcomb, K. Srirengan, and C. Chapman. Evaluation of homogenization for global/local stress analysis of textile composites. *Composite Structures*, 31:137–149, 1995.

[15] S.V. Lomov, D.S. Ivanov, I. Verpoest, M. Zako, T. Kurashiki, H. Nakai, and S. Hirosawa. Meso-fe modelling of textile composites : Road map, data flow and algorithms. *Composite Science and Technology*, 67:1870–1891, 2007.

[16] I. Verpoest and S.V. Lomov. Virtual textile composites software *WiseTex* : Integration with micro-mechanical, permeability and structural analysis. *Composite Science and Technology*, 65:2563–2574, 2005.

[17] G. Couegnat. *Approche multiechelle du comportement mecanique de materiaux composites a renfort tisse*. PhD thesis, Universite Bordeaux 1, 2008.

[18] G. Couegnat, E. Martin, J. Lamon, and N. Carrere. Multiscale modelling of the mechanical behaviour of woven composite materials. In *Proceedings of ICCM17, Edinburgh*, 2009.

[19] G. Perie, S.V. Lomov, I. Verpoest, and D. Marsal. Meso-scale modelling and homogenization of interlock reinforced composite. In *Proceedings of ICCM17, Edinburgh*, 2009.

[20] J. Schneider, G. Hello, Z. Aboura, M.L. Benzeggagh, and D. Marsal. A meso-fe voxel model of an interlock woven composite. In *Proceedings of ICCM17, Edinburgh*, 2009.

[21] S. Daggumati, W. Van Paepegem, J. Degrieck, J. Xu, S.V. Lomov, and I. Verpoest. Local damage in a 5-harness satin weave composite under static tension: Part ii – meso-fe modelling. *Composites Science and Technology*, 71:1217–1224, 2011.

[22] B.N. Cox, M.S. Dadkhah, W.L. Morris, and J.G. Flintoff. Failure mechanisms of 3d woven composites in tension, compression, and bending. *Acta Metallurgica et Materialia*, 42(12):3967–3984, 1994.

[23] R. Bohm, M. Gude, and W. Hufenbach. A phenomenologically based damage model for textile composites with crimped reinforcement. *Composites Science and Technology*, 70:81–87, 2010.

[24] X.L. Gao and K. Li. Damaged mosaic laminate model of woven fabric composites with transverse yarn cracking and interface debonding. *Composites Science and Technology*, 62:1821–1834, 2002.

[25] X.L. Gao, K. Li, and S. Mall. A mechanics-of-materials model for predicting young's modulus of damaged woven fabric composites involving three damage modes. *International Journal of Solids and Structures*, 40:981–999, 2003.

[26] A. Bensoussan, J. L. Lions, and G. Papanicolaou. *Asymptotic analysis for periodic structures.* North-Holland Publishing Company, 1978.

[27] P. Suquet. *Elements of homogenization for inelastic solid mechanics. In: Homogenization techniques for composite media.*, volume 272. Springer-Verlag, Berlin, 1987.

[28] R. H. J. Peerlings and N. A. Fleck. Computational evaluation of strain gradient elasticity constants. *International Journal for Multiscale Computational Engineering*, 2(4):599–619, 2004.

[29] A. L. Kalamkarov, I. V. Andrianov, and V. V. Danishevs'kyy. Asymptotic homogenization of composite materials and structures. *Applied Mechanics Reviews*, 62(3), 2009. Article Number: 030802.

[30] P. Cartraud and T. Messager. Computational homogenization of periodic beam-like structures. *International Journal of Solids and Structures*, 43(3–4):686–696, 2006.

[31] K. S. Challagulla, A. Georgiades, G. C. Saha, and A. L. Kalamkarov. Micromechanical analysis of grid-reinforced thin composite generally orthotropic shells. *Composites Part B-Engineering*, 39(4):627–644, 2008.

[32] A. Cecchi and K. Sab. A comparison between a 3D discrete model and two homogenised plate models for periodic elastic brickwork. *International Journal of Solids and Structures*, 41(9–10):2259–2276, 2004.

[33] A. Cecchi and K. Sab. A homogenized Reissner-Mindlin model for orthotropic periodic plates: Application to brickwork panels. *International Journal of Solids and Structures*, 44(18–19):6055–6079, 2007.

[34] A. Ibrahimbegovic and D. Markovic. Strong coupling methods in multi-phase and multi-scale modeling of inelastic behavior of heterogeneous structures. *Computer Methods in Applied Mechanics and Engineering*, 192(28–30):3089–3107, 2003.

[35] S. Ghosh, K. Lee, and P. Raghavan. A multi-level computational model for multi-scale damage analysis in composite and porous materials. *International Journal of Solids and Structures*, 38(14):2335–2385, 2001.

[36] P. Raghavan and S. Ghosh. A continuum damage mechanics model for unidirectional composites undergoing interfacial debonding. *Mechanics of Materials*, 37:955–979, 2005.

[37] J. R. Jain and S. Ghosh. Damage evolution in composites with a homogenization-based continuum damage mechanics model. *International Journal of Damage Mechanics*, 18(6):533–568, 2009.

[38] R. J. M. Smit, W. A. M. Brekelmans, and H. E. H. Meijer. Prediction of the mechanical behavior of nonlinear heterogeneous systems by multi-level finite element modeling. *Computer Methods in Applied Mechanics and Engineering*, 155(1–2):181–192, 1998.

[39] F. Feyel and J. L. Chaboche. FE^2 multiscale approach for modelling the elastoviscoplastic behaviour of long fiber SiC/Ti composite materials. *Computer Methods in Applied Mechanics and Engineering*, 183(3–4):309–330, 2000.

[40] V. G. Kouznetsova, W. A. M. Brekelmans, and F. P. T. Baaijens. An approach to micro-macro modeling of heterogeneous materials. *Computational Mechanics*, 27(1):37–48, 2001.

[41] M. G. D. Geers, V. G. Kouznetsova, and W. A. M. Brekelmans. Multi-scale computational homogenization: Trends and challenges. *Journal of Computational and Applied Mathematics*, 234(7):2175–2182, 2010.

[42] M.J. Pindera, H. Khatam, A.S. Drago, and Y. Bansal. Micromechanics of spatially uniform heterogeneous media: A critical review and emerging approaches. *Composites: Part B*, 40:349–378, 2009.

[43] M. G. D. Geers, E. W. C. Coenen, and V. G. Kouznetsova. Multi-scale computational homogenization of structured thin sheets. *Modelling*

and Simulation in Materials Science and Engineering, 15(4):S393–S404, 2007.

[44] E. W. C. Coenen, V. G. Kouznetsova, and M. G. D. Geers. A multi-scale computational strategy for structured thin sheets. *International Journal of Material Forming*, 1(Suppl.):61–64, 2008.

[45] E. W. C. Coenen, V. G. Kouznetsova, and M. G. D. Geers. Computational homogenization for heterogeneous thin sheets. *International Journal for Numerical Methods in Engineering*, 83(8–9):1180–1205, 2010.

[46] M. Mistler, A. Anthoine, and C. Butenweg. In-plane and out-of-plane homogenisation of masonry. *Computers & Structures*, 85(17–18):1321–1330, 2007.

[47] B. C. N. Mercatoris, P. Bouillard, and T. J. Massart. Multi-scale detection of failure in planar masonry thin shells using computational homogenisation. *Engineering Fracture Mechanics*, 76(4):479–499, 2009.

[48] B. C. N. Mercatoris and T. J. Massart. A coupled two-scale computational scheme for the failure of periodic quasi-brittle thin planar shells and its application to masonry. *International Journal for Numerical Methods in Engineering*, 85:1177–1206, 2011.

[49] L. Onal and S. Adanur. Modeling of elastic, thermal, and strength/failure analysis of two-dimensional woven composites - a review. *Applied Mechanics Reviews*, 60:37–49, 2007.

[50] G. S.V. Lomov, D.S. Perie, D. Ivanov, and D. Verpoest, I.and Marsal. Modeling three-dimensional fabrics and three-dimensional reinforced composites: challenges and solutions. *Textile Research Journal*, 81(1):28–41, 2011.

[51] B.V. Sankar and R.V. Marrey. A unit-cell model of textile composite beams for predicting stiffness properties. *Composites Science and Technology*, 49:61–69, 1993.

[52] P.W. Chung and K.K. Tamma. Woven fabric composites - developments in engineering bounds, homogenization and applications. *International Journal for Numerical Methods in Engineering*, 45:1757–1790, 1999.

[53] D.S. Ivanov, S.V. Lomov, S.G. Ivanov, and I. Verpoest. Stress distribution in outer and inner plies of textile laminates and novel boundary conditions for unit cell analysis. *Composites: Part A*, 41:571–580, 2010.

[54] A. Anthoine. Derivation of the in-plane elastic characteristics of masonry through homogenization theory. *International Journal of Solids and Structures*, 32(2):137–163, 1995.

[55] B. C. N. Mercatoris and T. J. Massart. Assessment of periodic homogenization-based multiscale computational schemes for quasi-brittle structural failure. *International Journal for Multiscale Computational Engineering*, 7(2):153–170, 2009.

[56] J. Zeman and M. Šejnoha. From random microstructures to representative volume elements. *Modelling and Simulation in Materials Science and Engineering*, 15(4):S325–S335, 2007.

[57] T. J. Massart, R. H. J. Peerlings, and M. G. D. Geers. An enhanced multi-scale approach for masonry wall computations with localization of damage. *International Journal for Numerical Methods in Engineering*, 69(5):1022–1059, 2007.

[58] J.C. Chaboche F. Feyel. Fe2 multiscale approach for modelling the elastoviscoplastic behaviour of long fibre sic/ti composite materials. *Comput Methods Appl Mech Engrg*, 183:309–330, 2000.

[59] V. G. Kouznetsova, M. G. D. Geers, and W. A. M. Brekelmans. Multi-scale constitutive modelling of heterogeneous materials with a gradient-enhanced computational homogenization scheme. *International Journal for Numerical Methods in Engineering*, 54(8):1235–1260, 2002.

[60] J.A. Masson, P.E. Bourban, L. Carlsson, and J.-P. Mercier. *Composites matrice organique : constituants, procds, proprits, Traits des Matriaux volume 15*. Presses Polytechniques et Universitaires Romandes, 2004.

[61] J. van Rijswijk and H.E.N Bersee. Reactive processing of textile fiber-reinforced thermoplastic composites - an overview. *Composites: Part A*, 38:666–681, 2007.

[62] C. Steggall-Murphy, P. Simacek, S.G. Advani, S. Yarlagadda, and S. Walsh. A model for thermoplastic melt impregnation of fiber bundles

during consolidation of powder-impregnated continuous fiber composites. *Composites: Part A*, 41:93–100, 2010.

[63] B. Piezel. *Comportement et analyse multiéchelle d'un composite à renfort tissé tridimensionnel*. PhD thesis, Mines ParisTech, 2010.

[64] B. Piezel, L. Laiarinandrasana, E. Mansour, J. Renard, and A. Thionnet. Analyse experimentale d'un composite textile en vue d'une modelisation multiechelle. In *Proceedings of JNC 16*, 2009.

[65] P. Bade, E. Vidal-Salle, E. Maire, and P. Boisse. Simulation and tomography analysis of textile composite reinforcement deformation at the mesoscopic scale. *Composites Science and Technology*, 68:2433–2440, 2008.

[66] A. Gasser, P. Boisse, and S. Hanklar. Mechanical behaviour of dry fabric reinforcements. 3d simulations versus biaxial tests. *Computational Materials Science*, 17:7–20, 2000.

[67] A. Marcellan, A. Bunsell, R. Piques, and Ph. Colomban. Micromechanisms, mechanical behaviour and probabilistic fracture analysis of pa 66 fibres. *Journal of Materials Science*, 38:2117–2123, 2003.

[68] A. Marcellan, Ph. Colomban, and A. Bunsell. (nano)structure, skin/core and tension behaviour of polyamide fibres. *Journal of Raman Spectroscopy*, 35:308–315, 2004.

[69] J.M. Herrera Ramirez, Ph. Colomban, and A. Bunsell. Micro-raman study of the fatigue fracture and tensile behaviour of polyamide (pa 66) fibres. *Journal of Raman Spectroscopy*, 35:1063–1072, 2004.

[70] Ph. Colomban, J.M. Herrera Ramirez, R. Paquin, A. Marcellan, and A. Bunsell. Micro-raman study of the fatigue and fracture pa 66 fibres: Comparaison with single pet and pp fibres. *Engineering Fracture Mechanics*, 73:2463–2475, 2006.

[71] Ph. Colomban. Nanomechanics of advanced polymer fibres. *Composites Science and Technology*, 69:1437–1441, 2009.

[72] J. Besson, G. Cailletaud, J.L. Chaboche, and S. Forest. *Mécanique non linéaire des matériaux*. Hermès, 2001.

[73] J. Lemaitre and J.L. Chaboche. *Mécanique des matériaux solides*. Dunod, 1985.

[74] C. Chamis. Mechanics of composite materials: past, present and future. *Journal of Composites Technology and Research*, 11:3–14, 1989.

[75] P. Badel, E. Vidal-Salllé, and P. Boisse. Rate constitutive equations for computational analyses of textile compsoite reinforcement mechanical behaviour during forming. *Composites: Part A*, 40:997–1007, 2009.

[76] M.C. Watson and T.W. Clyne. The tensioned push-out test for fibre-matrix interface characterisation under mixed mode loading. *Materials Science and Engineering*, 160:1–5, 1993.

[77] H. Zhang, M.L. Ericson, J. Varna, and L.A. Berglund. Transverse single-fibre test for interfacial debonding in composites : 1. experimental observations. *Composites: Part A*, 28:309–315, 1997.

[78] P. Lawrence. Some theoretical considerations of fibre pull-out from an elastic matrix. *Journal of Materials Science*, 7:1–6, 1972.

[79] P.S. Chua and M.R. Piggott. The glass fibre-polymer interface : I-theoritical consideration for single fibre pull-out tests. *Composites Science and Technology*, 22:33–42, 1985.

[80] C. Di Francia, T.C. Ward, and R.O. Claus. The single-fibre pull-out test. 1.: Review and interpretation. *Composites: Part A*, 27:597–612, 1996.

[81] P. Wriggers, G. Zavarise, and T. I. Zodhi. A computational study of interfacial debonding damage in fibrous composite materials. *Computational Materials Science*, 12:39–56, 1998.

[82] D.S. Li and M.R. Wisnom. Factors controlling the transverse tensile properties of unidirectional sic / ti-6al-4v. *Composites Engineering*, 5:235–255, 1995.

[83] A. Thionnet and J. Renard. Multi-scale analysis to determine fibre/matrix debonding criteria in sic/titanium composites with and without consideration of the manufacturing residual stresses. *Composites Science and technology*, 58:945–955, 1998.

[84] J. Besson and R. Foerch. Large scale object oriented finite element code design. *Computer Methods in Applied Mechanics and Engineering*, 142:165–187, 1997.

[85] B. Miller, U. Gaur, and D. E. Hirt. Measurement and mechanical aspects of the microbond pull-out technique for obtaining fiber/resin interfacial shear strength. *Composites Science and Technology*, 42:207–219, 1991.

[86] C.Y. Yue, H.C. Looi, and M.Y. Quek. Assessment of fibre-matrix adhesion and interfacial properties using the pull-out test. *International Journal of Adhesion and Adhesives*, 15:73–80, 1995.

[87] C.Y. Yue and H.C. Looi. Factors which influence the reliability of the assessment of interfacial bonding in fibrous composites using the pull-ou test. *International Journal of Adhesion and Adhesives*, 21:309–323, 2001.

[88] M. Brahmakumar, C. Pavithran, and R.M. Pillai. Coconut fibre reinforced polyethylene composites: effect of natural waxy surface layer of the fibre on fibre/matrix interfacial bonding and strength of composites. *Composites Science and Technology*, 65:563–569, 2005.

[89] B.A. Cheeseman and T.A. Bogetti. Ballistic impact into fabric and compliant composite laminates. *Composite Structures*, 61:161–173, 2003.

[90] B. Piezel, L. Laiarinandrasana, E. Mansour, and A. Thionnet. Analyse multiechelle d'un composite textile. In *Proceedings of JNC 16*, 2009.

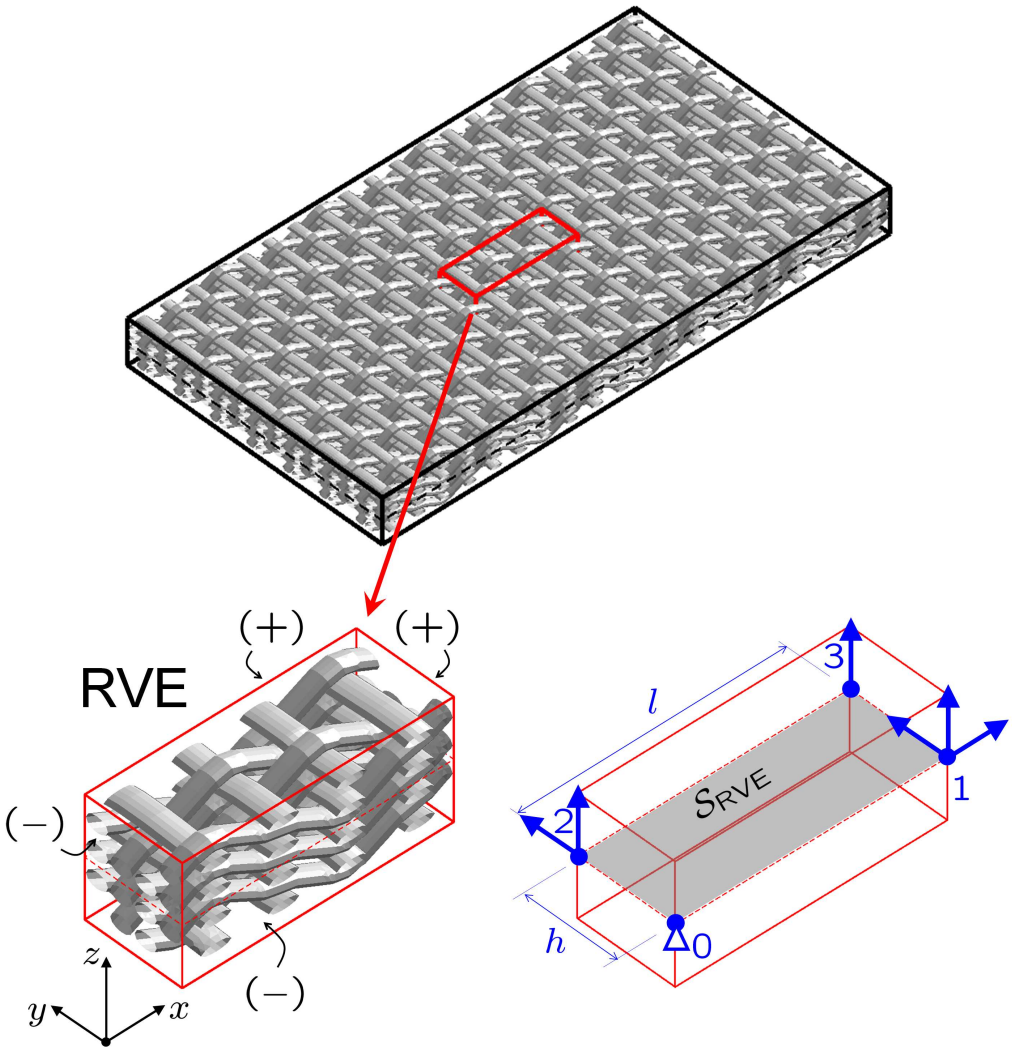

Figure 1: Rectangular parallelepipedic through-thickness RVE for three-dimensional woven composite: (left) woven fabric pattern and opposite internal boundaries, (right) controlling degrees of freedom and in-plane dimensions.

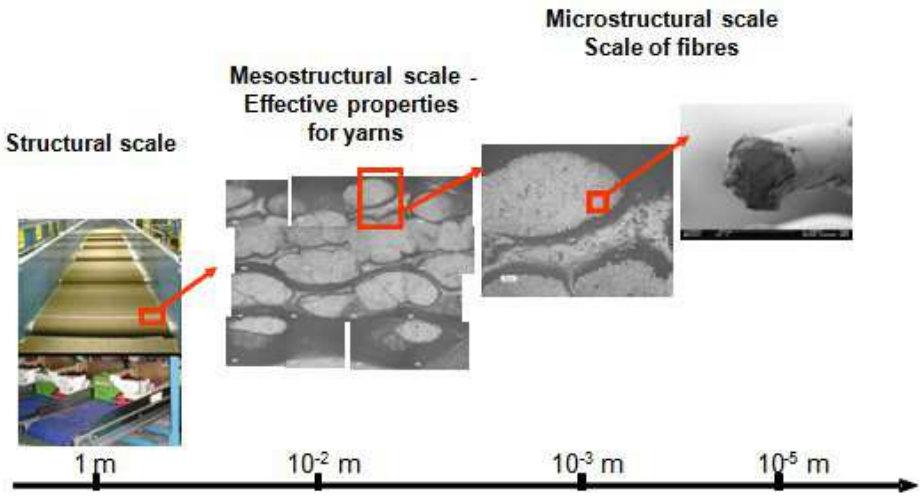

Figure 2: Multiscale structure of the 3D woven composite studied.

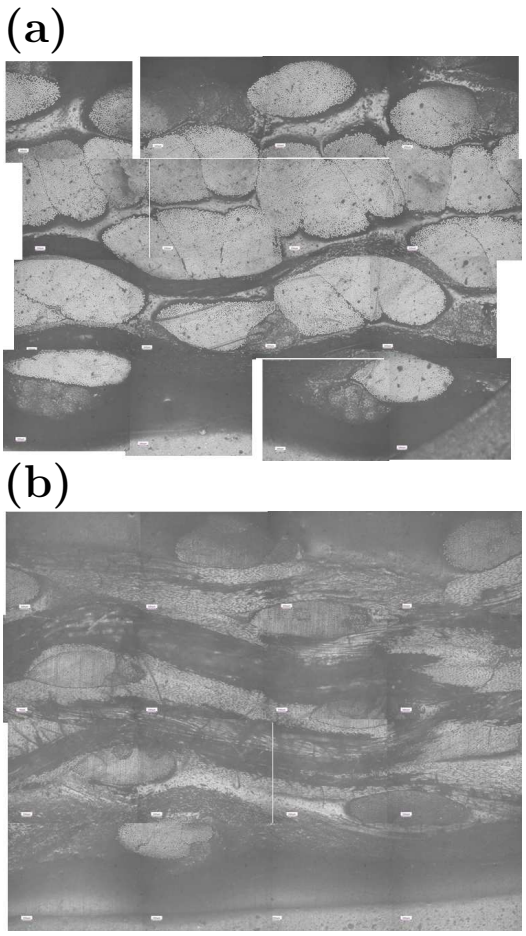

Figure 3: Transverse cutting of the textile composite (a) in the warp direction and (b) in the weft direction [90, 63].

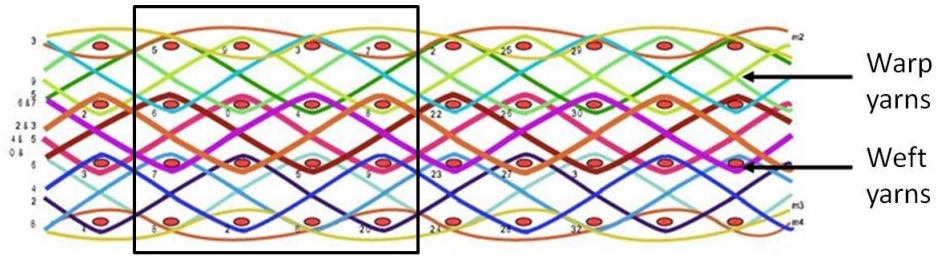

Figure 4: Representation of the fabric pattern [63].

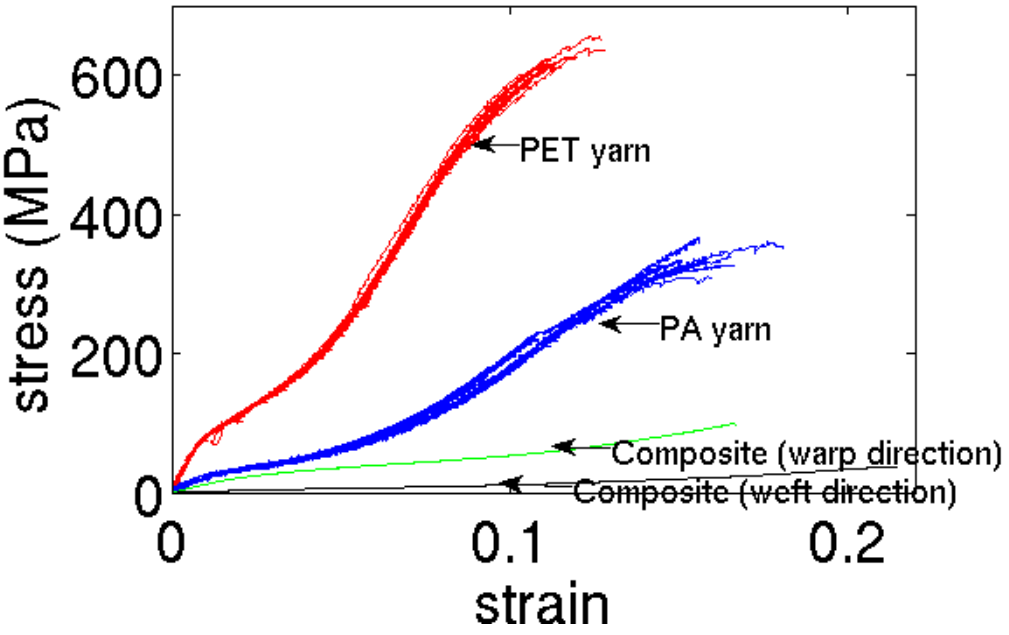

Figure 5: Monotonic tensile tests on the composite and on the yarns.

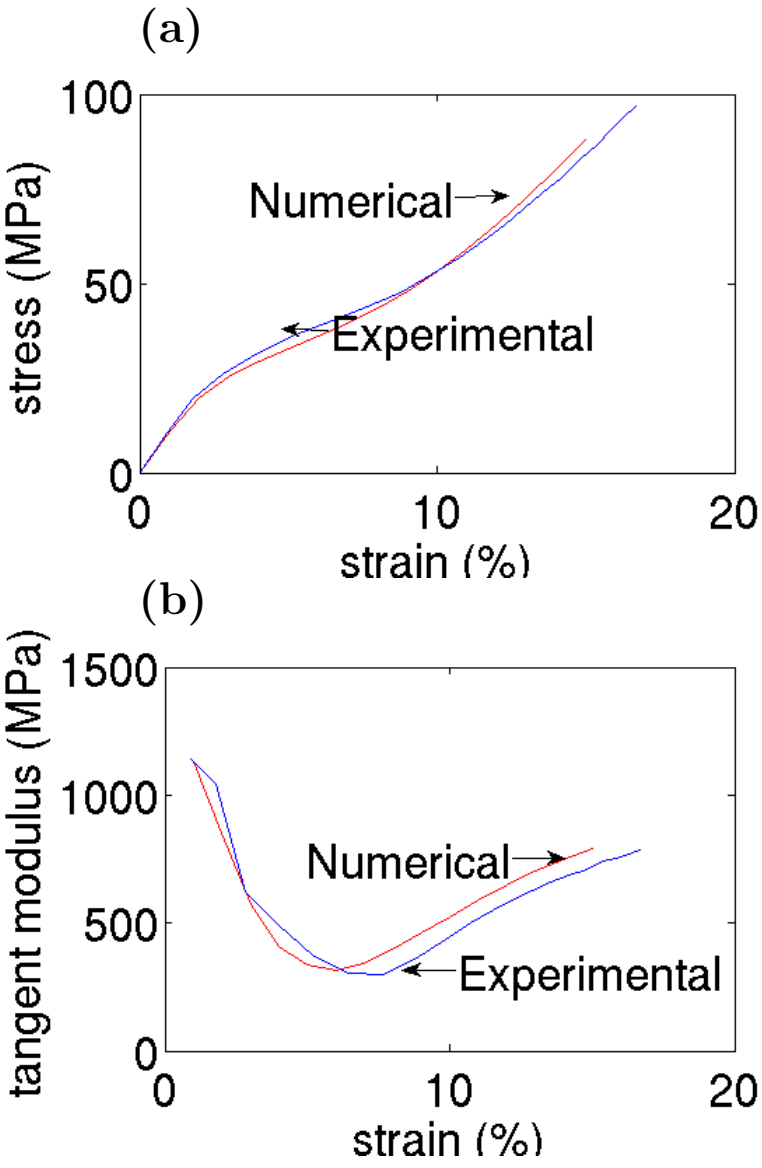

Figure 6: Macroscopic behaviour of the composite in the direction of warp yarns (a) macroscopic scale stress-strain response and (b) evolution of the tangent modulus with strain

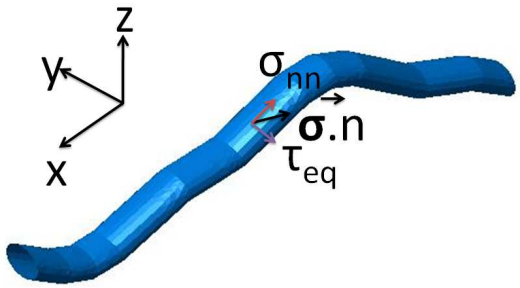

Figure 7: Definition of the normal and tangential components of the stress vector at the yarns/matrix interface.

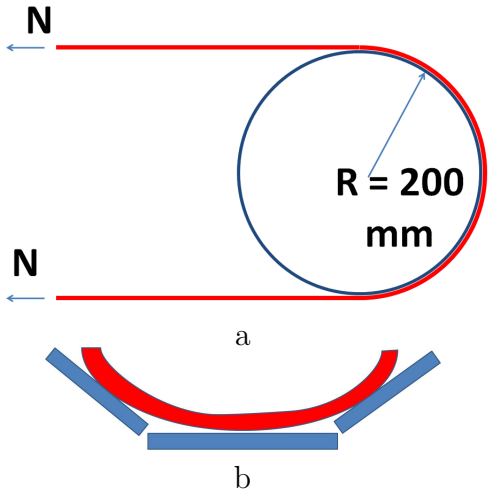

Figure 8: Typical loading modes of a transport moving strip : (a) longitudinal bending around a conveyor pulley with a pre-tension (b) transversal bending.

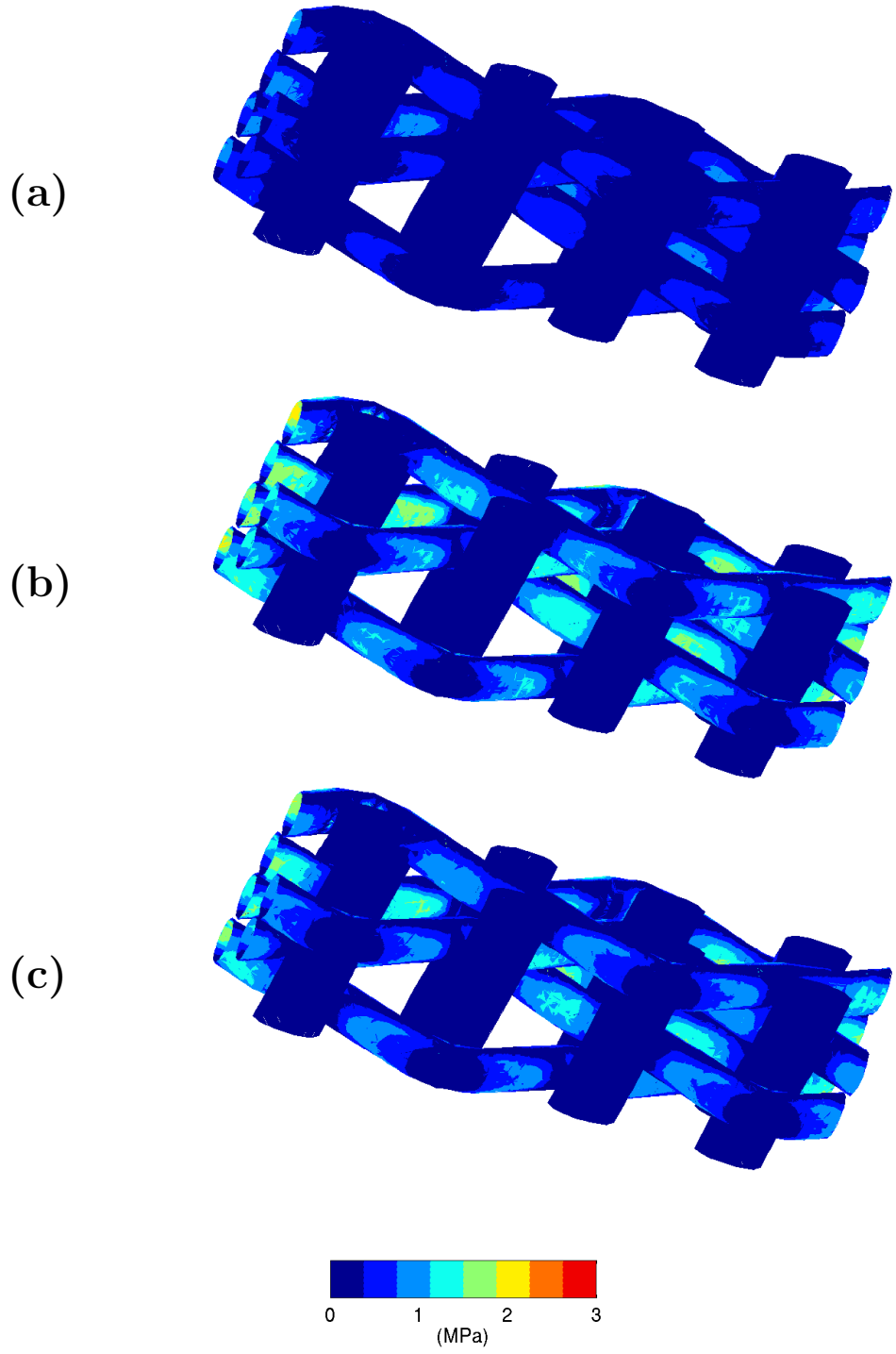

Figure 9: Stress state at the yarns - matrix interface for in-plane tension along the warp direction corresponding to a pre-tension of the composite (case LM1) : (a) normal (peeling) stress σ_{nn}, (b) tangential stress τ_{eq}, (c) delamination stress defined by (28) with $\alpha = 0.5$.

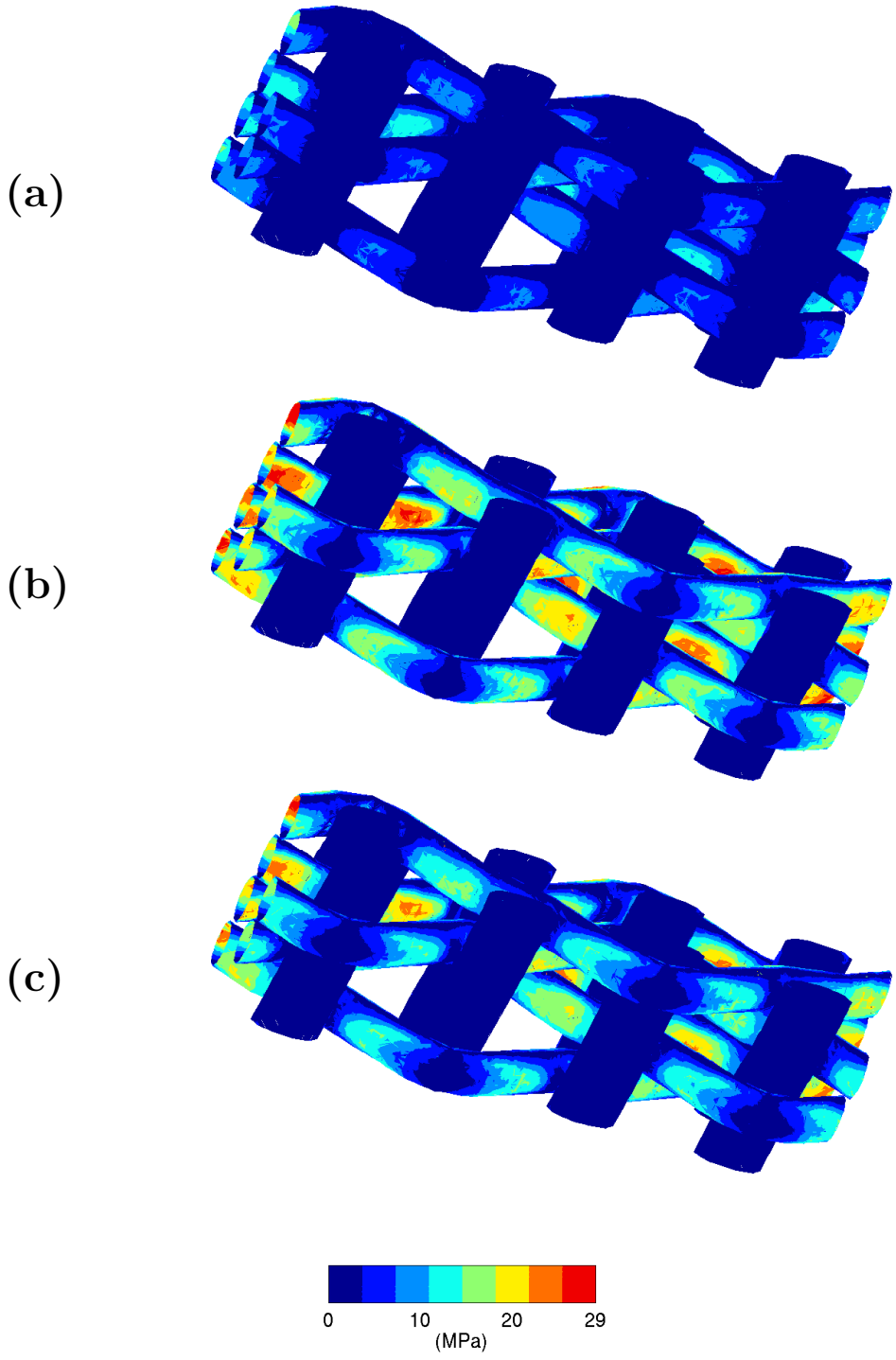

Figure 10: Stress state at the yarns - matrix interface for in-plane tension along the warp direction (case LM2) : (a) normal (peeling) stress σ_{nn}, (b) tangential stress τ_{eq}, (c) delamination stress defined by (28) with $\alpha = 0.5$.

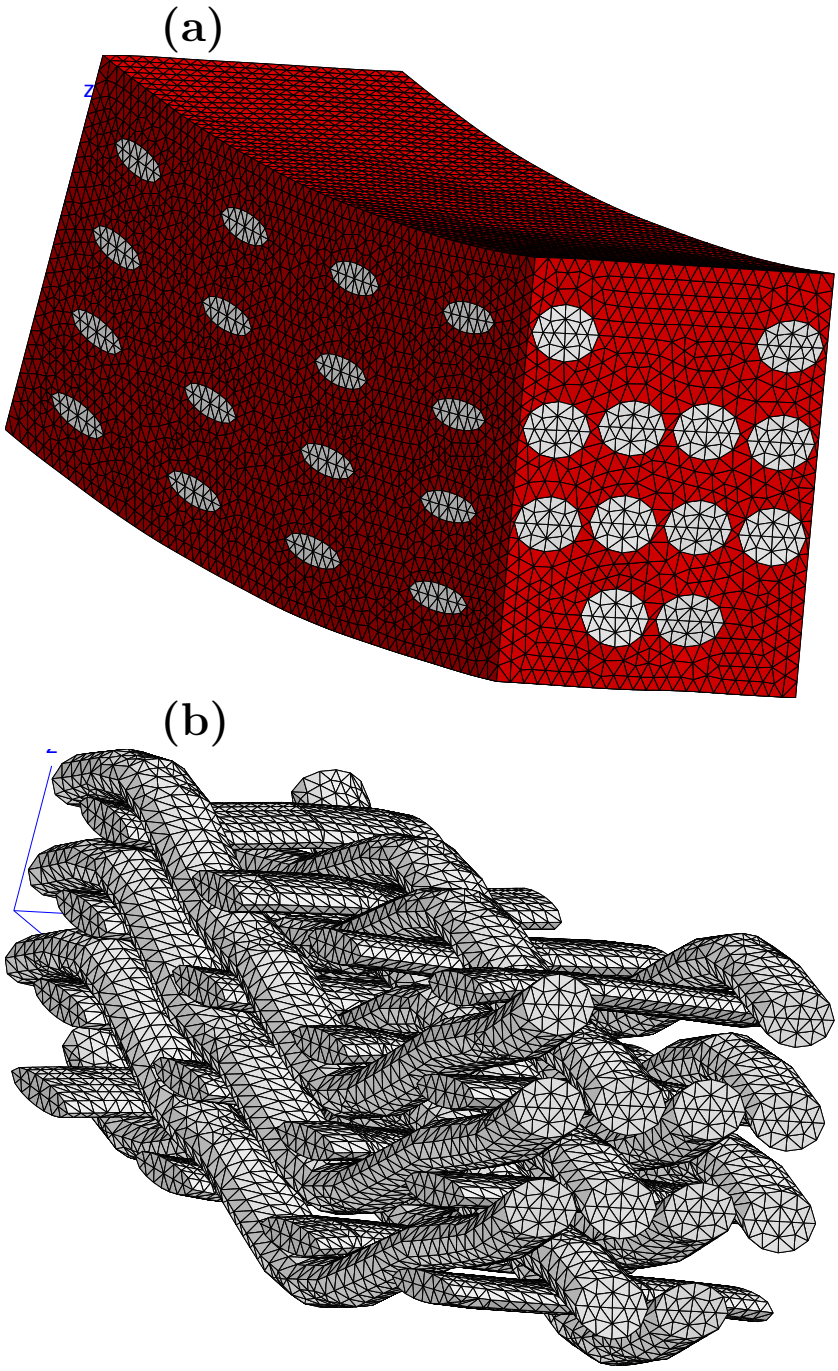

Figure 11: Deformed mesh for in-plane tension along the warp direction combined with bending (the displacements are magnified by a factor of 3) : (a) RVE, (b) Woven fabric.

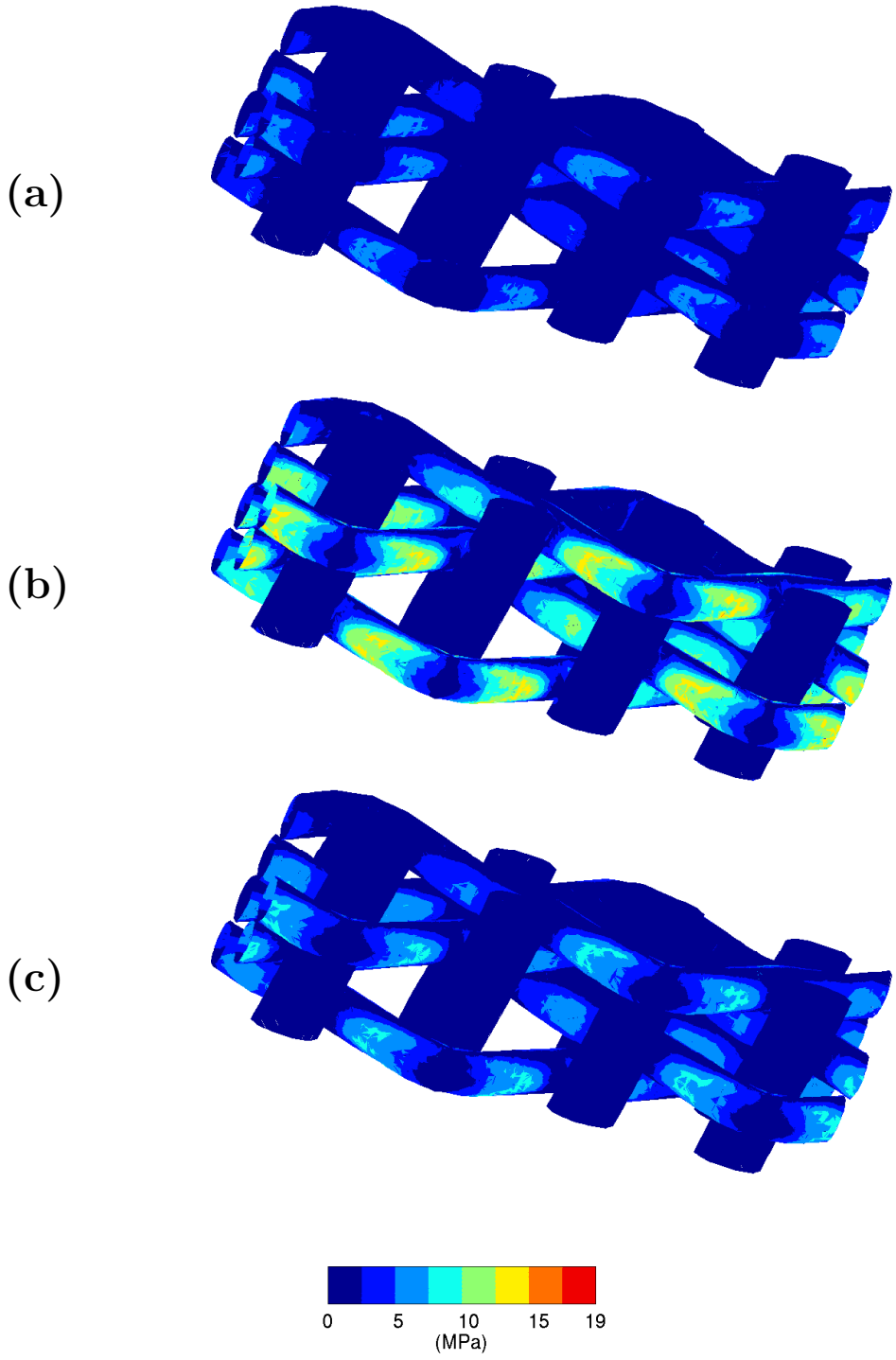

Figure 12: Stress state at the yarns - matrix interface for in-plane tension along the warp direction combined with bending (case LM3) : (a) normal (peeling) stress σ_{nn}, (b) tangential stress τ_{eq}, (c) delamination stress defined by (28) with $\alpha = 0.5$.

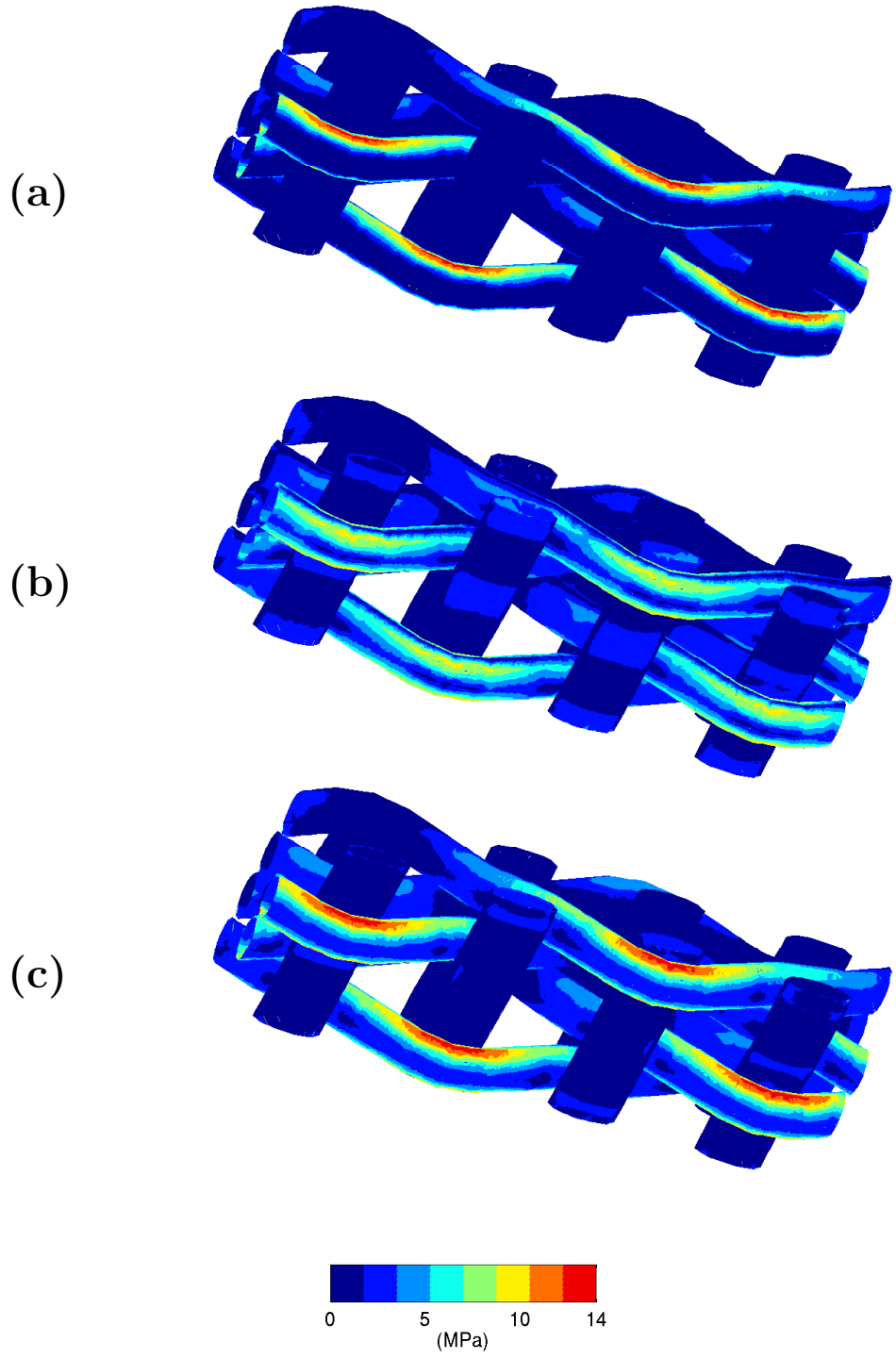

Figure 13: Stress state at the yarns - matrix interface for in-plane tension along the warp direction combined with a curvature χ_{yy} (case LM4) : (a) normal (peeling) stress σ_{nn}, (b) tangential stress τ_{eq}, (c) delamination stress defined by (28) with $\alpha = 0.5$.

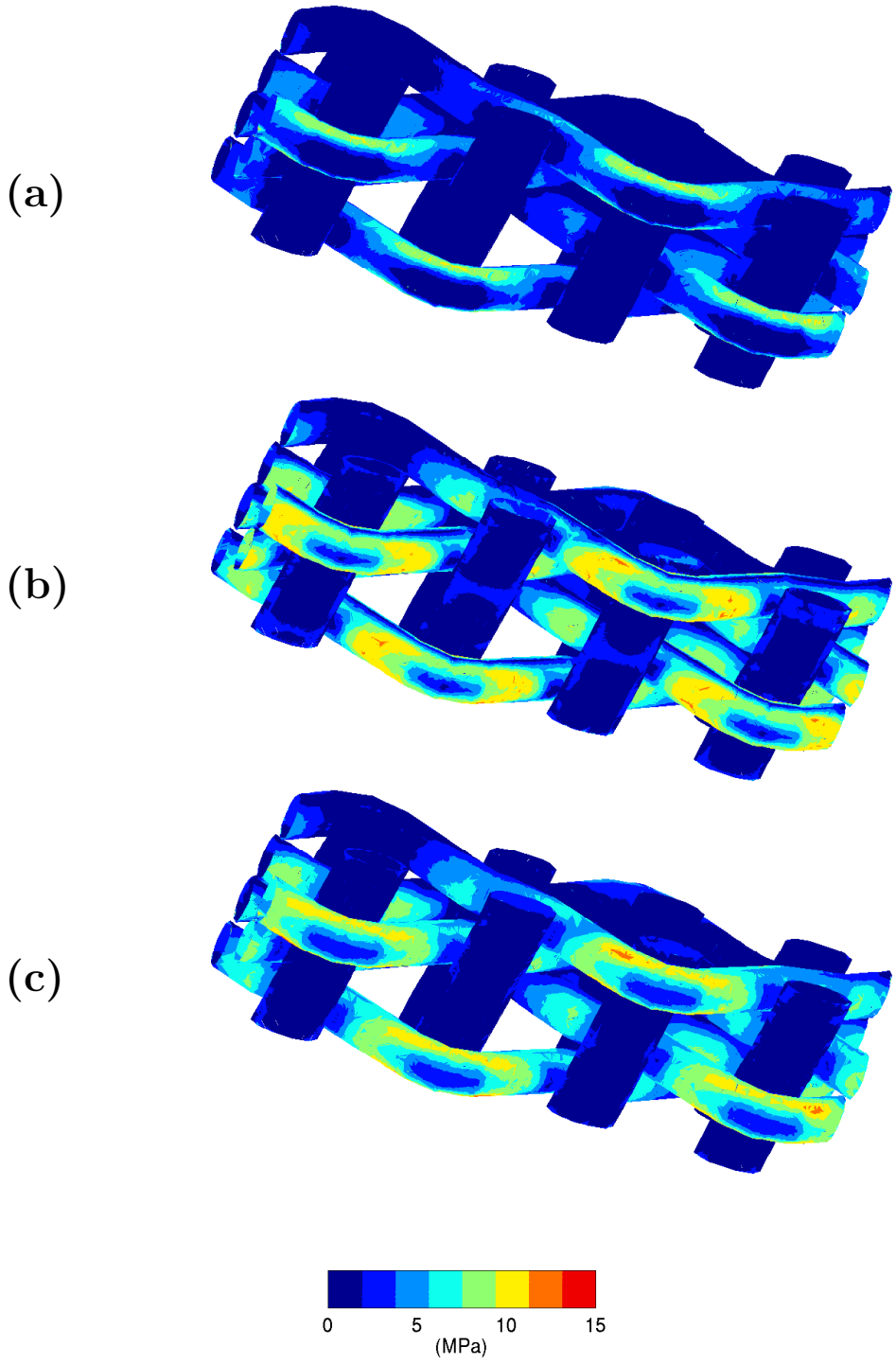

Figure 14: Stress state at the yarns - matrix interface for in-plane tension along the warp direction combined with a vertical impact (case LM5) : (a) normal (peeling) stress σ_{nn}, (b) tangential stress τ_{eq}, (c) delamination stress defined by 28 with $\alpha = 0.5$.

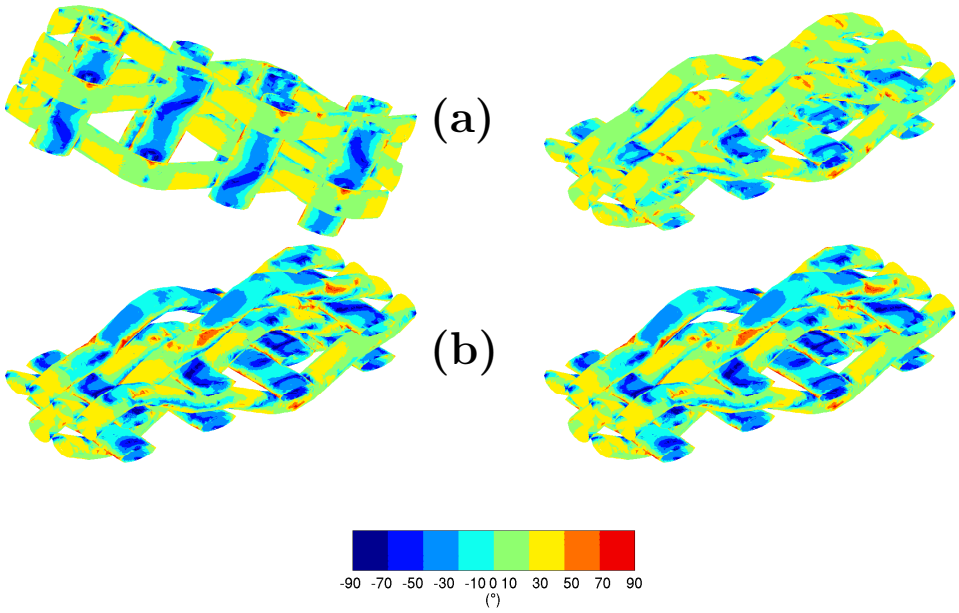

Figure 15: Phase-angle ψ fields at the yarns - matrix interface for in-plane tension along the warp direction (a) and for a curvature χ_{xx} (b) . The same distributions are plotted from different points of view to ease visualisation.

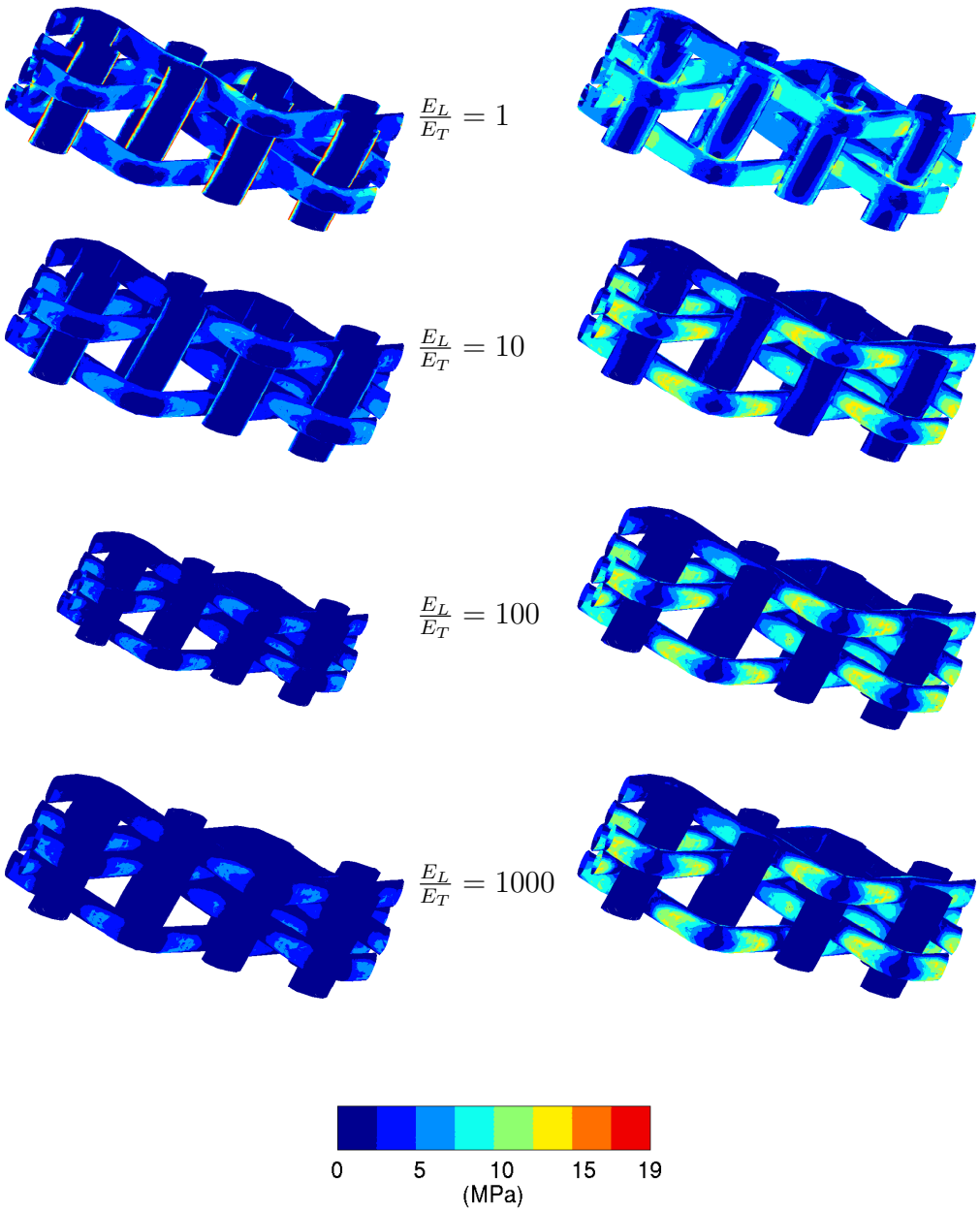

Figure 16: Influence of the ratio of longitudinal to transverse moduli in yarns on the stress levels at the interface between the yarns and the matrix: (left) normal (peeling) stress σ_{nn}, (right) tangential stress τ_{eq}